Environmental Nanotechnology, Monitoring & Management 15 (2021) 100414

Contents lists available at ScienceDirect

Environmental Nanotechnology, Monitoring & Management

journal homepage: www.elsevier.com/locate/enmm

Adsorptive removal of pollutants from industrial wastewater using mesoporous kaolin and kaolin/TiO_2 nanoadsorbents

S Mustapha [a,c,*], JO Tijani [a,c], MM Ndamitso [a,c], AS Abdulkareem [b,c], DT Shuaib [d], A. K Mohammed [e]

[a] Department of Chemistry, Federal University of Technology, PMB 65, Bosso Campus, Minna, Nigeria
[b] Department of Chemical Engineering, Federal University of Technology, PMB 65, Gidan Kwano Campus, Minna, Niger State, Nigeria
[c] Nanotechnology Research group, Africa Center of Excellence for Mycotoxin and Food Safety, Federal University of Technology, Minna, PMB 65, Niger State, Nigeria
[d] Department of Chemistry, Illinois Institute of Technology, 3101 S Dearborn Street, Chicago, IL 60616, USA
[e] Department of Chemistry and Biochemistry, North Carolina Central University, 1801 Fayetteville Street, Durham, North Carolina, 27707, USA

ARTICLE INFO

Keywords:
Kaolin
Adsorption
Kinetics
Avrami model
Spontaneous

ABSTRACT

This study evaluated the adsorption of some pollutants and water quality indicator parameters from tannery wastewater using natural kaolin and synthesized kaolin-TiO_2 nanocomposites. Natural kaolin, TiO_2 and kaolin with TiO_2 were characterized by X-ray diffraction (XRD), nitrogen gas adsorption-desorption Brunauer-Emmett-Teller (BET), Fourier Transform Infrared (FTIR), High Resolution Scanning Electron Microscopy (HRSEM), Energy Dispersive Spectroscopy (EDX), Selective Area Electron Diffraction (SAED) and High Resolution Transmission Electron Microscopy (HRTEM). The results of the characterization showed addition of TiO_2 nanoparticles onto kaolin influenced the particle morphology, phase identification, surface area and functional groups. Batch adsorption techniques were investigated under the influence of contact time, adsorbent dosage and temperature. The adsorption trend of the parameters onto the nanoadsorbents was in the order kaolin/TiO_2>kaolin. Kaolin/TiO_2 nanoadsorbent with surface area of 53.80 m^2/g showed high adsorption potentials for pollutants removal. Several adsorption isotherm and kinetic model were investigated. The adsorption data fitted well to pseudo-second order kinetic model. It was found that increase in temperature correspond to increase in the adsorption of the pollutants and other parameters, indicating that the system was endothermic in nature. From the results obtained, it can be concluded that the kaolin-TiO_2 nanocomposites is a promising nanoadsorbent for the adsorption of toxic pollutants in tannery wastewater than kaolin alone.

1. Introduction

In the last couple of years, population growth, migration, increasing urbanization, industrialization and climate change have influenced the supply and demand chain for freshwater resources. According to United Nations Department of Economic and Social Affairs (UNDESA, 2013), the world population is projected to reach 9.1 billion by 2050, and it is estimated that more than 2.4 billion people living in Sub-Saharan Africa (SSA) will be without access to sustainable water resources. In Nigeria, more than 63 million people do not have access to safe water, and thousands of the populace have resulted in consumption of unconventional water. This unsatisfactory report from water pollution shows that citizens are vulnerable to diseases such as typhoid, polio, cholera and dysentery (WHO, 2016). Among various organic and inorganic contaminants discharged into the environment, potentially toxic metals (PTM) also known as heavy metals have been identified as a possible cause of human diseases. The sources of heavy metals in water bodies include electroplating, mining, smelting, pharmaceuticals, battery manufacturing, textile and tannery industries. Specifically, tanning activities generates almost forty million litres of wastewater yearly, containing constituents such as chromium, chloride, lime with high dissolved salt and other contaminants (Ahmed et al., 2016). In most developing countries like Nigeria, tanning industries discharged wastewater without proper treatment into the sewage system have detrimental effects fauna and flora. Therefore, removal of toxic pollutants especially chromium and other related toxic metals in tannery wastewater is considered imperative.

Different techniques such as chemical precipitation (Byambaa et al.,

* Corresponding author at: Department of Chemistry, Federal University of Technology, PMB 65, Bosso Campus, Minna, Nigeria.
E-mail address: saheedmustapha09@gmail.com (S. Mustapha).

https://doi.org/10.1016/j.enmm.2020.100414
Received 28 February 2020; Received in revised form 4 December 2020; Accepted 17 December 2020
Available online 29 December 2020

2018), solvent extraction (2017), ozonation (Ma et al., 2018), flotation (Antonyová and Antony, 2017), membrane separation (Brito et al., 2019), reverse osmosis (Thaçi and Gashi, 2019) have been used for treatment of tannery wastewater. However, in spite of their prolific use, these methods are expensive, inadequate for removal of heavy metals in the range of 1–100 mg/L. Therefore, adsorption technology has become an ideal method for the removal of toxic contaminants from wastewater due to its simplicity, high efficiency, economical value and environmental friendliness. The use of nanoadsorbents for adsorption of pollutants is found to have unique properties applied in modern material sciences research (Burakov et al., 2018). The procedures involved in the production of these nanoscale based materials include chemical, physical, irradiation, and biological methods and have resulted in environmental pollution. Therefore, the quest for clean, safe, eco-friendly, and less or nontoxic techniques for the synthesis of nanoparticles is desirable.

Titanium oxide (TiO_2) has been considered a non-toxic nanomaterial with a high concentration of hydroxyl groups, due to its chemical and photochemical stability (Qian et al., 2012). TiO_2 nanoparticles can be prepared sol-gel, hydrothermal, precipitation, chemical vapour deposition, microemulsion, laser ablation, thermal decomposition of organometallic precursor among others. Among these, the sol-gel method has been found to be the most outstanding due to the generation of high-quality surface morphologies (Sharma et al., 2014). Titanium dioxide nanoparticles have been utilized in industrial and commercial applications for solar cells, memory devices, adsorption of pollutants and wastewater purifications (Liu et al., 2014; Lu et al., 2017).

In recent times, the application of titanium dioxide (TiO_2) has attracted much attention in the treatment of wastewater (Dariania et al., 2016; Lin et al., 2018; Tijani et al., 2019). Although numerous investigations have been carried out on the practical applications of these nanoparticles, some setbacks such as aggregation in the fluidized system, low surface area, separation from the treated water and fate in wastewater treatment were identified (Dale et al., 2015; Lofrano et al., 2016). Researchers have continued to search for appropriate support materials to improve the efficiency of TiO_2. For instance, Belver et al. (2016) worked on W-TiO_2 anchored on clay for removal of atrazine; TiO_2 nanoparticles immobilized on mesoporous silica for removal of dyes from wastewater by Maučec et al. (2017), TiO_2 nanoparticles immobilized on macroporous clay-alumina as support for the removal of dye (Oun et al., 2017) and synthesized TiO_2/zeolite for the removal of methylene blue dye by Setthaya et al. (2017). Among various support materials, clay mineral called “kaolin” has shown some unique properties. Kaolin exhibits great advantages due to its high cation exchange capacity (CEC), chemical stability and low expansion coefficient (Uddin, 2016). Its favourable properties which include high specific area and charged layer also aid adsorption on the sites of the kaolinite. For example, polyacrylic acid kaolin composite was successfully used for the removal of heavy metals from water (Barbooti et al., 2019). Until now, studies have shown that nanocomposites have the large ability and potential in the treatment of wastewater especially for adsorption/photocatalyst but the use of TiO_2/kaolin nanocomposites for the removal of pollutants from tannery wastewater is limited. Therefore, kaolin is selected as supporting material for titania in this research.

This study report the preparation of kaolin-TiO_2 nanocomposite via a sol-gel process. In this instance, nanosized TiO_2 crystals were synthesized and immobilized on kaolin. In addition, the prepared materials were characterized using high-resolution scanning electron microscopy (HR-SEM), high-resolution transmission electron microscopy (HRTEM), Fourier-transformed infrared spectroscopy (FTIR), selective area electron diffraction (SAED) and energy dispersive X-ray (EDX) analysis. The kaolin and kaolin/TiO_2 nanoadsorbents were used for tannery wastewater treatment.

2. Experiment

2.1. Materials

Raw kaolin was obtained from a clay deposit in Gbako Local Government Area in Niger State, Nigeria. Titanium tetraisopropoxide (TTIP, 97 %), sodium hydroxide (NaOH, $\geq$ 97 %), ethanol ($\geq$ 99.5 %), acetic acid (CH_3COOH, $\geq$ 99.85 %), nitric acid (HNO_3, $>$ 90 %), sodium hypochlrite (NaOCl), ethylenediamine tetraacetic acid disodium salt dihydrate (EDTA 2Na.2H_2O), hydrogen peroxide (H_2O_2) and HCl (37 %) were procured from Sigma Aldrich. All the reagents/chemicals were analytical grade and used without further purification. Deionized water was used throughout the study.

2.2. Pre-treatment on natural kaolin

Natural kaolin was first pre-treated to remove residual impurities and improve its absorptive properties. A known volume (100.0 cm^3) of 0.5 M sodium hypochlorite solution was added to the prepared slurry (50 g clay and 200 cm^3 de-ionized water). The resultant mixture was decanted and 10.0 cm^3 of 0.5 M H_2O_2 was added for the further bleaching process. A suspension of kaolin (100 g/dm^3) was transferred into a jar filled with deionized water and stirred for 30 min for particle size screening. Afterwards, the mixture was allowed to settle for 24 h. Supernatant from the jar was decanted and filtered. The filtrate was oven-dried at 100 °C for 24 h until there was complete dryness.

2.3. Sol-gel synthesis of TiO_2 nanoparticles

TiO_2 nanoparticles were prepared using a sol-gel described as follow: About 10 cm^3 of TTIP was added to 100 cm^3 of the deionized water, thoroughly stirred for 15 min using magnetic stirrer. The pH of the sol was adjusted to 8 using 0.1 M of sodium hydroxide and then stirred continuously for 1 h. The resulting gell was washed with ethanol followed by deionized water for three successive times and filtered using Whatman filter paper. The synthesized nanoparticles were dried in an oven at 100 °C for 2 h and later calcined in a muffle furnace at 450 °C for 3 h.

2.4. Synthesis of kaolin supported TiO_2 nanoparticles

Kaolin supported TiO_2 nanoparticles were prepared by a wet impregnation method described as follow: About 5.0 g of the beneficiated kaolin was weighed and mixed with 2.0 g of TiO_2 prepared under the same condition in section 2.3; followed by addition of 20 cm^3 of deionized water and stirred at 150 rpm for 30 min. The resulting mixture (nanocomposite) was dried overnight in an oven at 100 °C, and later calcined at 450 °C for 3 h and then crushed to powder form for further analysis.

2.5. Characterization

Phase structure of the prepared materials was determined using powdered X-ray diffraction (PXRD) model Bruker AXS D8 Advance (USA) with Cu-Kα radiation. The surface morphologies of kaolin, titanium oxide and kaolin/titanium oxide nanocomposite were examined using a Zeiss Auriga HRSEM (USA). HRSEM coupled with Energy Dispersion Spectroscopy (EDS) was used to examine the elemental composition of the samples. The surface area, total pore volume and pore size of the materials were determined using a Brunauer-Emmett-Teller (BET), Novawin Quantachrome instrument. The FTIR analysis of the samples was conducted on Thermo Scientific Nicolet iS5 instrument with iD5 ATR spectrometer recorded at a wavenumber of 4000 cm^{-1} to 500 cm^{-1}.

2.6. Adsorption experiment

Batch adsorption experiments were performed in order to evaluate the equilibrium time, obtain adsorption kinetics, adsorption isotherm and adsorption thermodynamic data. The removal efficiency (% removal) and the adsorption capacity (q_e, mg/g) of kaolin and kaolin/TiO_2 nanocomposite of some physical and chemical indicators from tannery wastewater in mg/dm^{3}as seen in Table 1 were determined. The wastewater was filtered with a mesh size of 0.5 μm prior to batch adsorption experiment. The effects of contact time on the physical and chemical indicators analysed in this research work using kaolin and kaolin/TiO_2 nanocomposites were investigated by contacting 0.20 g of the adsorbents in each case, with 40 cm^3 of the wastewater in a corked 250 cm^3 Erlenmeyer flask, agitated at 150 rpm for 0, 5, 10, 15, 20, 25 and 30 min on an orbital shaker. The effects of adsorbent dosage on the equilibrium uptake of some physicochemical parameters were investigated with adsorbent doses of 0.4, 0.6, 0.8, 1.0, 1.2 and 1.4 g. The experiments were performed by adding the known weights of the adsorbents into 250 cm^3 flasks containing 40 cm^3 of the wastewater each. The flasks were shaken at 150 rpm at the optimum contact time while the temperature and pH of the solution were kept constant for each parameter studies. The effects of temperature on the equilibrium uptake of the indicator parameters from tannery wastewater by kaolin and kaolin/TiO_2 nanocomposites at the temperature values of 30, 40, 50, 60, 70 and 80 °C were investigated. The experiments were performed by adding 0.2 g of the adsorbent to 40 cm^3 of wastewater in 250 cm^3 conical flasks, shaken in a water bath at respective temperature for the optimum contact time. At the end of each experiment, the resulting solution was separated from the adsorbent using Whatman paper No. 42 and the residual concentration of physicochemical parameters were analysed using APHA, manual method (2005).

The known weight of adsorbent dosage was added to 40 cm^3 of the wastewater in 250 cm^3 erlenmeyer flask. The flask was placed on an orbital shaker, under the set conditions of contact time and shaking speed (150 rpm). The solution was filtered using Whatman No 42 and then transferred to glass tube for analysis. Pb, Cd and total Cr ion concentration of the solution before and after adsorption were determined using atomic absorption spectroscopy (Perkin Elmer A Analyst, 4000). All experiments were conducted in duplicate.

The removal efficiency (%) and the adsorption capacity (mg/g) of the parameter studied by the adsorbents under equilibrium time were computed using eqs. 1 and 2, respectively.

$$\%\ \text{Removal} = \frac{C_0 - C_e}{C_e} \times 100 \quad (1)$$

$$q_e = \frac{(C_0 - C_e)}{M} V \quad (2)$$

Where C_0 (mg/dm^3) and C_e (mg/dm^3) are the initial and equilibrium liquid phase concentration, respectively; V (dm^3) the volume of the solution and M (g) the mass of the adsorbent.

Table 1
Some physicochemical properties of tannery wastewater before adsorption.

Parameter	Recorded value
Colour	Dark brown
Odour	Objectionable
pH	5.84 ± 0.02
Chemical oxygen demand (COD) (mg/dm^3)	1988.60 ± 0.23
Biological oxygen demand (BOD) (mg/dm^3)	625.30 ± 0.10
Nitrate (mg/dm^3)	118.30 ± 0.16
Lead (mg/dm^3)	1.70 ± 0.13
Cadmium (mg/dm^3)	3.23 ± 0.50
Chromium (mg/dm^3)	8.30 ± 0.28

2.7. Desorption and regeneration studies

Desorption experiments of metal ions were performed to examine reusability. After adsorption of metal ions, nanoadsorbents were agitated in diluting agents such as 0.1 M HNO_3, 0.1 M CH_3COOH and deionized water. The nanoadsorbents were separated by centrifugation at 4000 rpm and then dried in an oven at 105 °C for 1 h. 0.2 *g* of the nanoadsorbents and 50 cm^3 of eluting agents were mixed in Erlenmeyer flask and agitated for respective optimum contact time for the metal ion. The desorbed nanoadsorbents were separated by filtration and the filtrate was used to obtain the desorbed metal ion concentrations. Desorption efficiency was calculated using Eq. (3).

$$D(\%) = \frac{M_d}{M_a} \times 100 \quad (3)$$

Where M_d is the quantity of desorbed metal and M_a is the quantity of adsorbed metal.

After desorption, the nanoadsorbents were washed with 0.1 M EDTA for regeneration. The adsorption-desorption cycle was repeated four more times to analyse the removal efficiency of nanoadsorbents.

3. Results and discussion

3.1. XRD studies

The phase structure and degree of crystallinity of the samples were analysed by XRD. Fig. 1 shows the XRD pattern of kaolin, anatase TiO_2 and kaolin/TiO_2 nanocomposites. The XRD diffraction patterns of kaolin according to the JCPDS file revealed the presence of diffraction peaks at 2θ value of 12.40°, 19.85°, 24.95°, 36.07°, 46.59°, 54.61° and 73.77° which correspond to the crystallographic orientation of (001), (020), (002), (200), (221), (150) and (402) respectively. Similar diffraction peaks were also reported by Zen et al. (2018). The kaolin sample showed the predominate phase as kaolinite and quartz, which are commonly found in kaolin.

The XRD patterns of TiO_2 exhibits several diffraction peaks at 2θ value of 25.28°, 37.80°, 48.05°, 53.89°, 55.06°, 62.90°, 68.76°, 70.31°, 75.03° and 82.66° index to the (101), (004), (112), (200), (105), (211), (204), (116), (220), (215) and (224) crystal planes of anatase phase titania (JCPDS 00−021-1272), respectively. The average size of anatase crystallites (D), calculated by the Scherrer's Eq. (4).

$$D = \frac{K\lambda}{\beta \cos\Theta} \quad (4)$$

Where D is the crystallite size of the particle, θ is the Bragg diffraction angle, β is the full width at half-maximum (FWHM), λ is the wavelength of Cukα (0.15418 nm) and k (0.94) is a constant.

In Fig. 1, it was noticed that the XRD pattern of kaolin-TiO_2 nanocomposites remains unchanged despite the addition of kaolin onto TiO_2 as the diffraction peaks common to kaolin at 2θ still persist. It was found that the diffraction peaks of kaolin overshadowed that of TiO_2 reflections, leaving the 2θ reflections of kaolinite phase unchanged. The observed peaks of anatase TiO_2 disappeared while the peaks of kaolinite still remained intact. This may be due to the followings: (i) the closeness of peaks of anatase to kaolin, making the TiO_2 phase to be difficult to identify (ii) the weakness and low-strength peaks of TiO_2 leading to non-generation of new peak and non-aggregation of the nanocomposite and (iii) the amount of TiO_2 nanoparticles is low to be detected by XRD. However, the (101) reflection peak of anatase in TiO_2/kaolin nanocomposite appears with a peak intensity at 25.28° as a result of TiO_2 incorporation. A similar trend was observed by Wongso et al. (2019), which stated that other diffraction peaks of TiO_2 were hidden by kaolin as a result of particle size of TiO_2 as compaed to kaolin. The low-strength peaks of calcined kaolin/TiO_2 indicated that the nanocomposites were decorated with well-crystallized TiO_2 nanoparticles. However, the

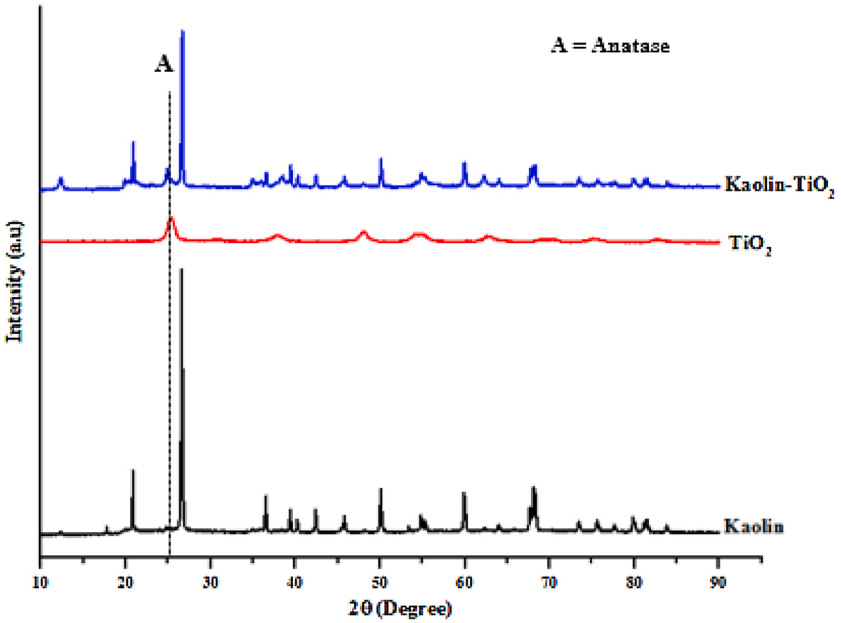

Fig. 1. XRD patterns for kaolin, TiO_2 and kaolin/TiO_2.

characteristic peaks of kaolinite were still retained, suggesting that the structure of the clay was not destroyed. It may be remarked that the characteristic peaks of anatase are very close to those from kaolinite, which make it difficult to analyse. The crystallite size of titania particles was computed via the Debye-Scherrer equation and the crystallite sizes were shown in Table 2.

3.2. Fourier transform infrared spectroscopy (FTIR) analysis

FTIR spectral analysis was performed to identify the crosslink in kaolin, TiO_2 and possible interaction between the nanocomposites (kaolin-TiO_2) (Fig. 2). The following characteristic bands appeared at 3694 cm^{-1}, 3648 cm^{-1} and 3400 cm^{-1} can be found in the kaolin which is assigned to the −OH stretching vibration, while the peak at 1636 cm^{-1} corresponds to H—OH— bending vibration. These peaks may be due to the bonding between atoms of oxygen and protons attached to aluminium ions in the octahedral structural layer. The peaks may also be linked to water physisorbed on the kaolin surface (Madejova, 2003). The bands at 1007 cm^{-1} for Si-O-Al, 692 cm^{-1} and 689 cm^{-1} for Si-O stretching, 912 cm^{-1} for Al−OH and the band at 796 cm^{-1} and 783 cm^{-1} attributed to the presence of quartz (Si-O). The band at 912 cm^{-1} could be ascribed to OH deformation of inner hydroxyl groups in the bonding of Al–Al−OH octahedral sheet of the kaolin.

The FTIR peaks for the TiO_2 indicate the presence of stretching vibration of Ti–O at 604 cm^{-1} and 657 cm^{-1}, stretching of Ti–O–Ti at 1470 cm^{-1}, stretching of Ti−OH at 1640 cm^{-1}), and stretching vibration of −OH at 3400 cm^{-1}. Comparing the spectra of kaolin/TiO_2 nanocomposite with that of kaolin and TiO_2 samples, it was found that a sharp peak at 930 cm^{-1} was ascribed to the stretching vibration of Si–O–Ti bond. Similar peaks were observed for both kaolin and kaolin/TiO_2 samples, which suggest the stronger intermolecular attraction between the kaolin and TiO_2 nanoparticles.

Table 2
Different angles and their corresponding *hkl* values with sizes of TiO_2 nanoparticles.

Angle	hkl	Size (nm)
25.28	101	2.01
37.80	004	1.75
38.58	112	7.35
48.05	200	2.07
53.89	105	1.02
55.06	211	0.77
62.90	204	1.05
68.76	116	0.61
70.31	220	2.77
75.03	215	0.43
82.66	224	3.37

3.3. HRSEM for kaolin, TiO_2 and kaolin-TiO_2

The results of the surface morphologies of kaolin, TiO_2 nanoparticles and kaolin/TiO_2 nanocomposite analysed by HRSEM depicted in Fig. 3. Fig. 3 (a) showed that kaolin contains a mixture of quartz and kaolin forming dense aggregates texture. It was observed that a smaller number of small flakes with the hexagonal structure were arranged in face-to-face patterns compared to well crystalline pseudohexagonal edges of kaolinite as well as plate-like edged kaolinite particles.

As it can be seen from the HRSEM images, Fig. 3 (b) showed the interparticle porosity of the mesoporous spherical TiO_2 nanocrystal. The spheroidal crystal morphologies of TiO_2 samples were clearly evident and well dispersed, homogeneous but agglomerated. In the case of Fig. 3 (c), less aggregated and well defined spherical particles structure was identified in the kaolin/TiO_2 nanocomposites. The addition of kaolin into the lattice layer of TiO_2 did not affect the shape TiO_2.

3.4. HRTEM for kaolin, TiO_2 and kaolin-TiO_2

Fig. 4 presents HRTEM and SAED analysis of kaolin, TiO_2 nanoparticles and kaolin/TiO_2 nanocomposite. The structure of kaolin revealed a pseudo-hexagonal structure of kaolinite (Fig. 4 (A_1-A_3). The presence of cross-fringes indicates the edge observation that the internetwork layers are coherently stacked and the stacking is ordered more within those domains. SAED result of the kaolin showed the turbostratic patterns over the aggregated amorphous kaolin that were randomly oriented on each other. This indicates that the particles were kaolinite phase and the dotted concentric rings (Fig. 4A_3) were assigned to quartz and halloysite forms. The EDX spectra revealed the existence of the following elements: O, Al, Si, K, Ti and Fe (Table 3).

Fig. 4 (B_1-B_3) revealed the HRTEM images of TiO_2 nanoparticles revealed anomalistic spherical crystals of TiO_2 with average particle size

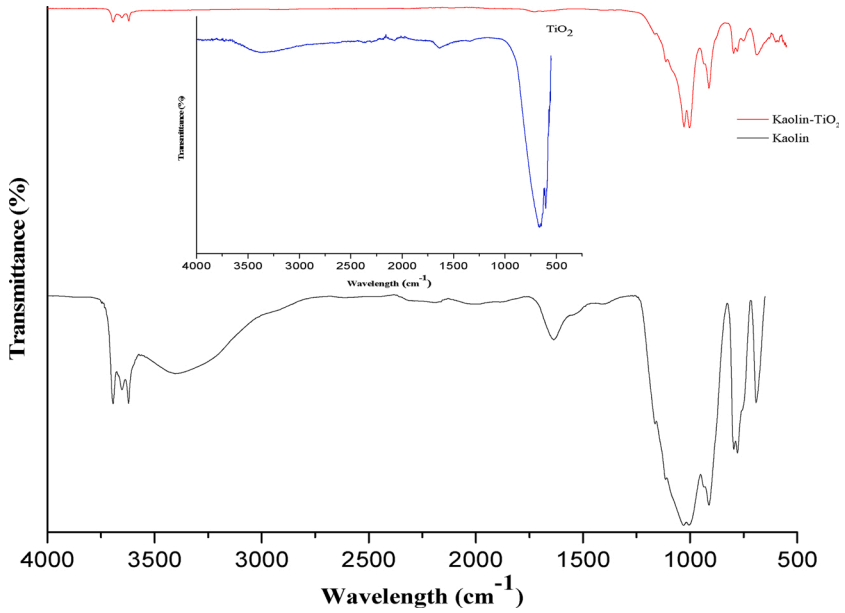

Fig. 2. FTIR spectra for TiO_2 (inlet), kaolin and kaolin/TiO_2.

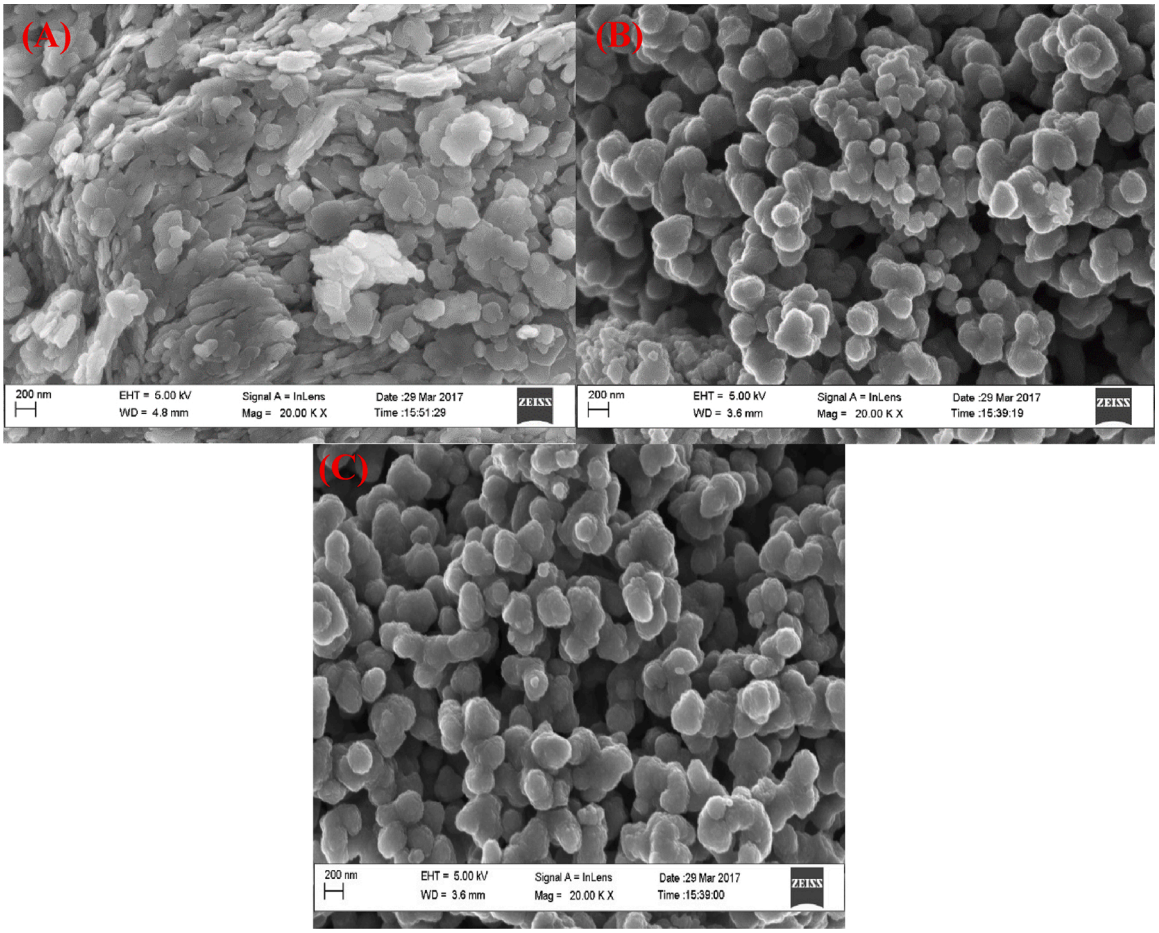

Fig. 3. HRSEM images of (A) beneficiated kaolin (B) TiO_2 nanoparticles and (C) kaolin/TiO_2 nanocomposite at 450 °C.

ranges between 10–14.30 nm, which is in good agreement with XRD results. Lattice fringes were observed in HRTEM shown in Plate II (B_2), with that d-spacing of 0.35 nm, 0.24 nm ad 0.23 nm for TiO_2 planes of (101), (004) and (112), respectively. These correspond to the result obtained from XRD patterns.

The EDX spectrum of TiO_2 nanoparticles revealed the presence of Ti, O, C, and Ni for the as-synthesized TiO_2 (Table 3). The presence of oxygen was due to the interaction of TiO_2 with air during synthesis

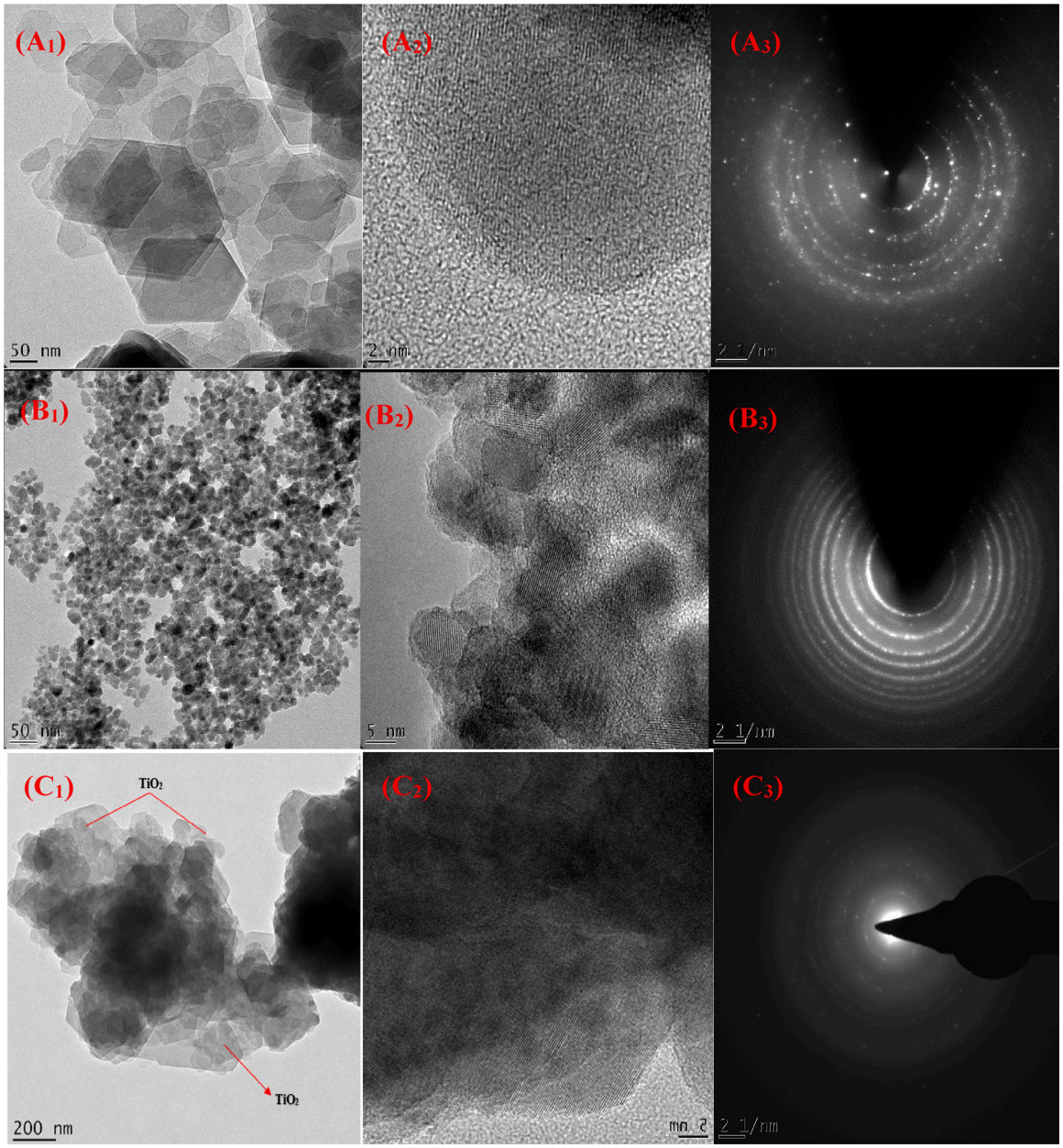

Fig. 4. HRTEM and SAED Analysis of kaolin (A1-A3), TiO_2 nanoparticles (B1-B3) and kaolin/TiO_2 nanocomposite (C1-C3) calcined at 450 °C.

Table 3
EDX results in atomic and weight percentage of beneficiated kaolin, TiO_2 nanoparticle and kaolin/TiO_2 nanocomposites.

Element	Kaolin		TiO_2		Kaolin-TiO_2	
	Weight	Atomic	Weight	Atomic	Weight	Atomic
O	52.96	66.83	17.9	31.29	33.21	50.28
Al	18.84	14.09	–	–	18.86	16.93
Si	24.71	17.77	–	–	24.54	21.17
Ti	0.74	0.32	60.86	35.54	20.53	10.39
Fe	2.74	0.99	–	–	2.86	1.24
C	–	–	9.53	22.2	–	–
Ni	–	–	4.42	2.11	–	–
Na	–	–	7.3	8.86	–	–

(washing with ethanol and water) and calcination process. The observed peaks of Na originated from NaOH while the spectrum of C was from the carbon holey grid used for the HRTEM analysis. The selected area of electron diffraction (SAED) analysis in Fig. 4 (B2) indicated that the TiO_2 nanoparticles were polycrystalline due to the presence of dotted concentric rings.

The HRTEM analysis of TiO_2/kaolin nanocomposites in Fig. 4 (C_1-C_3) reveals that dispersion/distribution of spherical TiO_2 nanoparticles in kaolin having lattice spacing of 0.35 nm, a characteristic peak for (101) crystal plane of anatase phase of TiO_2. Similar result has also been reported on TiO_2 nanoparticles immobilized on clay by Mishra et al. (2017). The HRTEM analysis further confirmed that TIO_2 nanoparticles were both anchored on the internal and the external layer of the kaolin, which may increase the active binding sites required for the adsorption process. Additionally, EDX measurement analysis performed on the nanocomposites inTable 3 showed the existence of some elements from the nanoparticles and the kaolin.

3.5. BET analysis

The quasi-overlapping adsorption-desorption curves and the pore

size distribution of beneficiated kaolin, TiO_2 nanoparticle and kaolin-TiO_2 nanocomposite are presented in Fig. 5 (a–c). The N_2 adsorption-desorption isotherm curve of the sample can be classified as Type IV, which belong to a Type H3 hysteresis loop indicating a slight mesoporous material with small pore size. The BET specific surface area, pore volume and pore diameter of kaolin according to Barrette-Joyner-Halenda method were 17 m^2/g, 0.018 cm^3/g and 3.587 nm respectively. This shows that beneficiated kaolin is mesoporous.

The specific area and pore size distribution of the as-synthesized TiO_2 sample are characterized using the nitrogen adsorption-desorption isotherm measurement. The BET and BJH methods were used to analyse the surface area and pore size distribution. According to the International Union of Pure and Applied Chemistry (IUPAC), the N_2 adsorption-desorption isotherm exhibit Type IV hysteresis isotherm for the as-synthesized TiO_2 showed that the nanoparticles are mesoporous. The adsorption hysteresis approached the region of relative pressure (P/P_o) above 0.9 with the BET of the mesoporous TiO_2, 43.80 m^2/g, pore volume of 0.024 cm^3/g and smaller pores, 4.053 nm (as seen in Table 4).

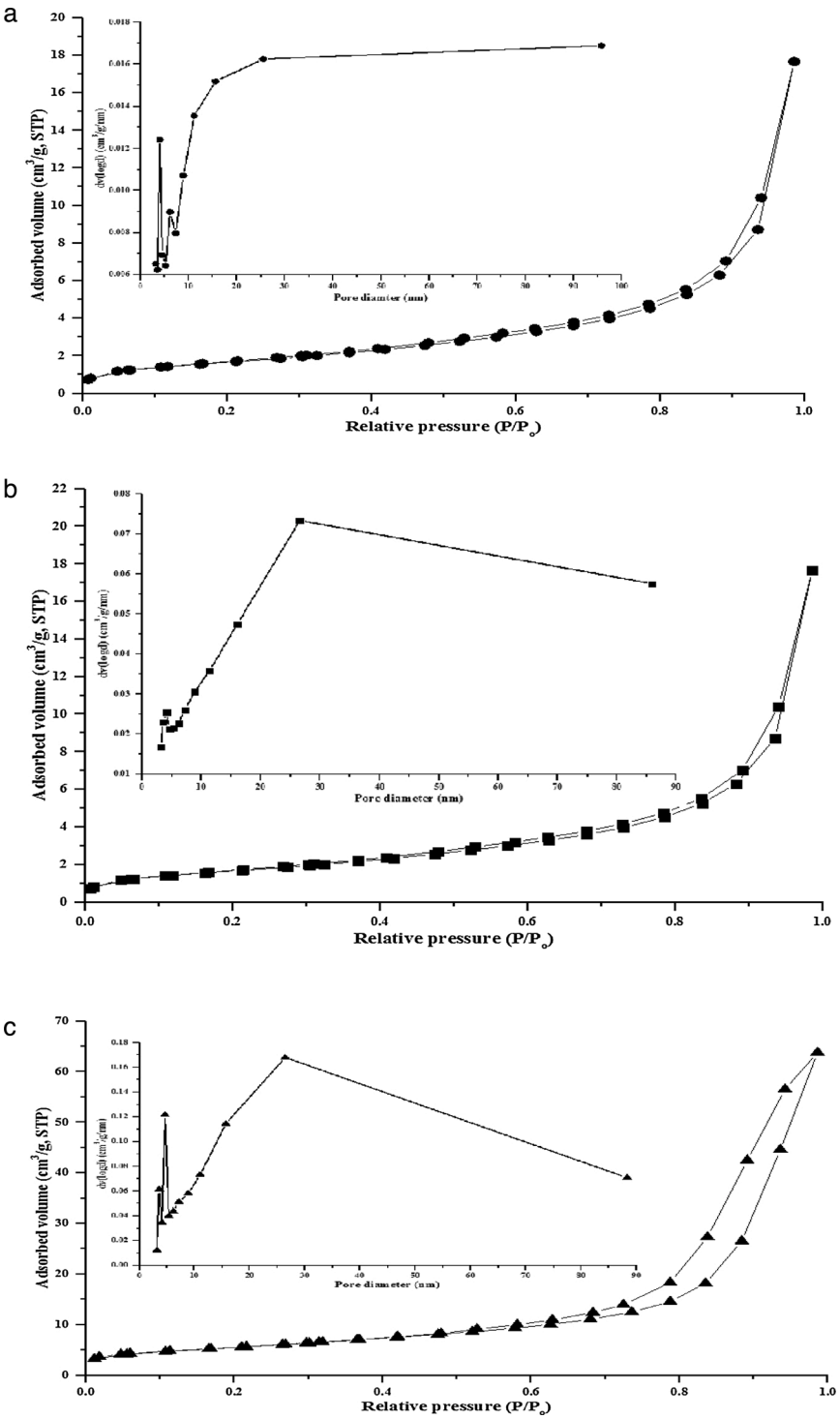

Fig. 5. a. Adsorption-desorption curve and pore size distribution (inlet) of kaolin. b. Adsorption-desorption curve and pore distribution (inlet) of TiO_2 nanoparticles. c. Adsorption-desorption curve and pore size distribution of kaolin/TiO_2 nanocomposite.

Table 4
The comparison of specific surface area, pore volume and pore size of the kaolin, TiO_2 nanoparticles and kaolin/TiO_2 nanocomposites.

Properties	Kaolin	TiO_2	Kaolin/TiO_2
Surface area (m^2/g)	17.00	43.80	53.80
Pore volume (cm^3/g)	0.018	0.024	0.070
Pore diameter (nm)	3.587	4.053	5.214
Phase	Kaolinite	Anatase	Kaolinite/anatase

Moreover, the distribution shows that the porosity of the TiO_2 is contributed by the mesoporosity possibly due to its nature.

The N_2 adsorption-desorption isotherm of the TiO_2/kaolin nanocomposite exhibited Type IV isotherm with H3 hysteresis loops, an indication of mesoporosity according to the IUPAC (Fig. 5c). The BET and BJH pore size distributions correspond to mesoporous. The nanocomposite result showed that BET specific surface area and pore volume 53.80 m^2/g and 0.070 cm^3/g, respectively. As previously reported by Mishra (2017) and Wongso et al. (2019), the surfaces of kaolin and kaolin/TiO_2 obtained were lower compared to the present study. As shown in Table 4, it was noted that the kaolin/TiO_2 nanocomposites has a higher surface area than the beneficiated clay and TiO_2 nanoparticles. A similar finding was observed by (Mishra, 2017) and Wongso et al. (2019). This implied that TiO_2 nanoparticles have been incorporated successfully to the interlayers of the clay surface, thereby responsible for the increased surface area, pore volume and pore size. The mesoporosity could allow different molecules of different sizes into their pores, making the nanocomposites highly suitable for adsorption purposes. The specific surface area of the nanocomposites is greater than the beneficiated kaolin. The high BET values are attributed to an increase in pore volume and pore size.

3.6. Adsorption studies

3.6.1. Effect of contact time

The effect of contact time on the adsorption of the toxic pollutants in wastewater onto the adsorbent is important in order to achieve equilibrium adsorption. The influence of contact time on the adsorption of COD, BOD and nitrate onto kaolin and kaolin/TiO_2 was shown in Fig. 6 While the adsorption of Pb, Cd and Cr onto the adsorbents is as shown in Fig. 7. The rate of adsorption was faster at the initial but becomes slow on reaching the equilibrium. Different equilibrium times were observed for all the parameters on the adsorbents. The maximum percentage adsorption of Pb, nitrate, COD, Cd, Cr and BOD onto kaolin was 57.65, 61.46, 72.81, 59.35, 53.01 and 82.65 % at equilibrium time of 5, 10, 15, 15, 15 and 20 min, respectively. For kaolin/TiO_2 nanocomposite, the equilibrium percentage adsorption of COD, BOD, Cr, Pb, Cd and nitrate

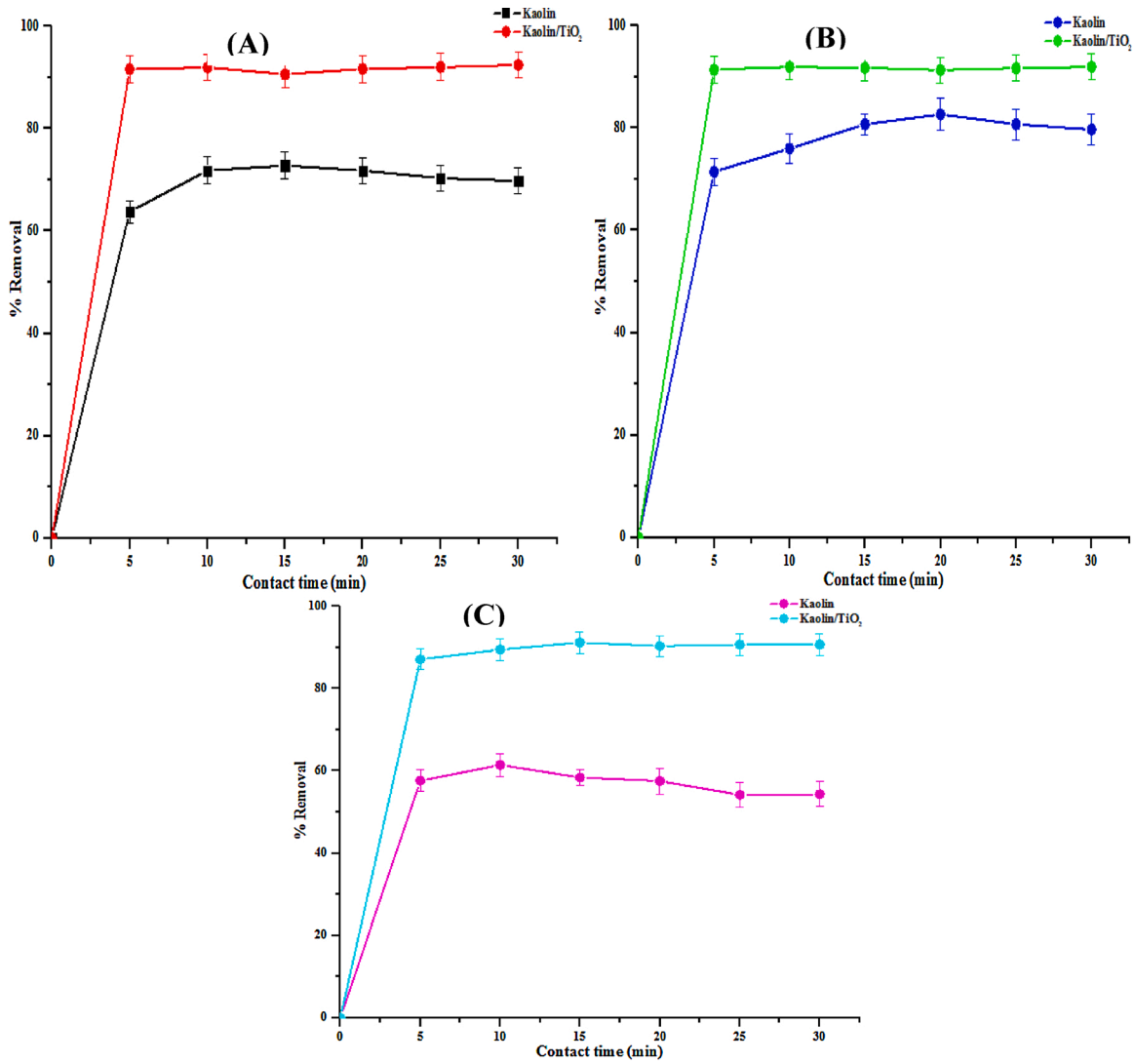

Fig. 6. Effect of contact time on percentage removal of (A) COD (B) BOD and (C) nitrate onto beneficiated kaolin and kaolin/TiO_2 nanocomposite (conditions: adsorbent dose 0.2 g, agitation speed 150 rpm, temperature 29 °C).

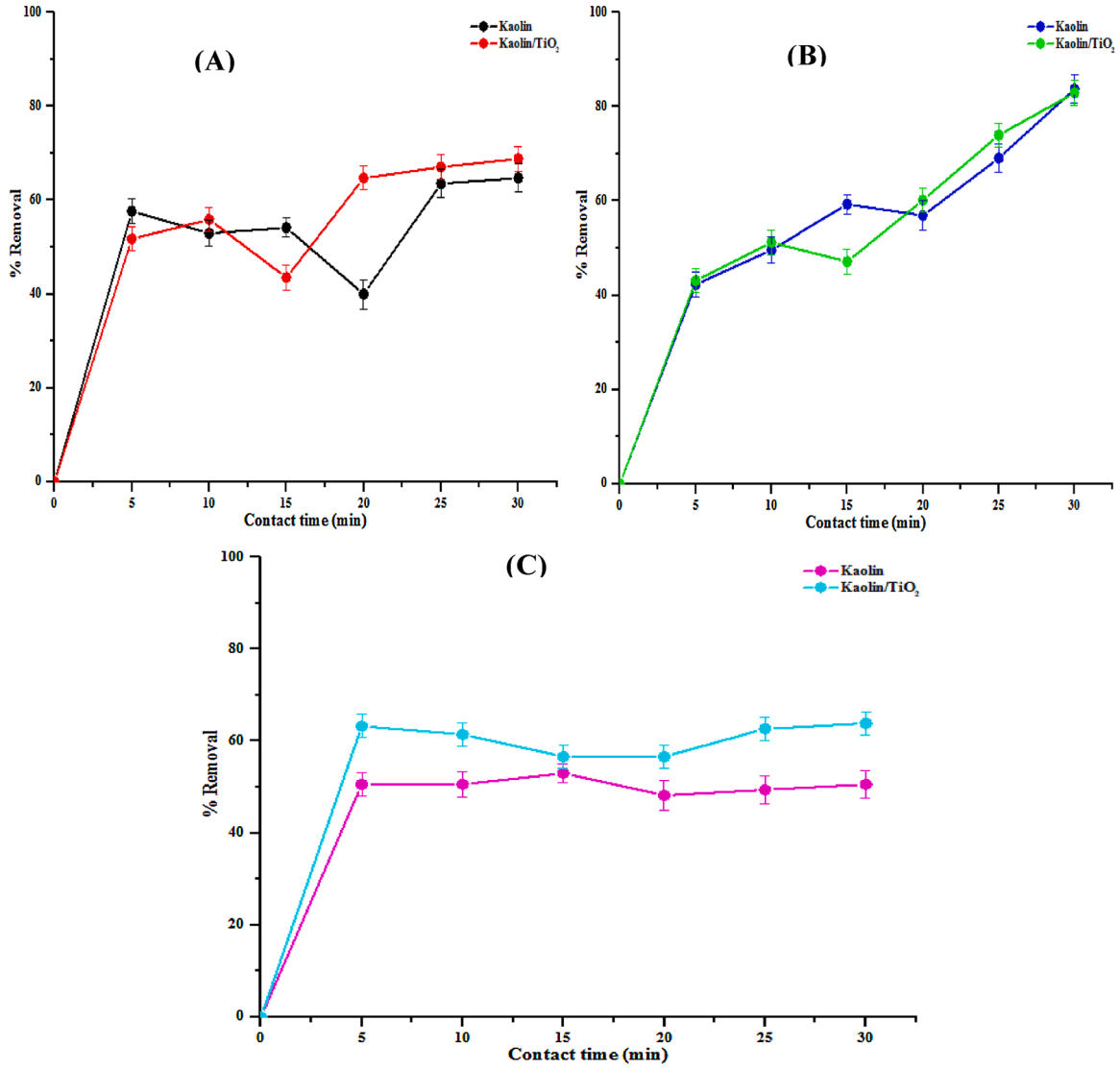

Fig. 7. Effect of contact time on percentage removal of (A) Pb (B) Cd and (C) Cr onto beneficiated kaolin and kaolin/TiO_2 nanocomposite (conditions: adsorbent dose 0.2 g, agitation speed 150 rpm, temperature 29 °C).

was 91.95, 91.93, 63.25, 55.88, 51.22 and 91.19 % at the optimum time of 10, 10, 5, 10, 10 and 15 min, respectively. Also, the equilibrium was attained faster for COD, BOD and nitrate adsorption using kaolin/TiO_2 while the equilibrium for Pb, Cd and Cr removal was fast using kaolin. It was observed that adsorption rate was rapid, eventhough different optimum times were observed under the same adsorbent usage. This could be attributed to the availability of the active/binding sites on the adsorbents. It was found that on reaching the optimum time/equilibrium, the rate of adsorption equals the rate of desorption. Zulfikar et al. (2016) observed a similar trend when investigating removal of humic acid using Fe_2O_3-chitosan hydrid nanoparticles from solution. They noticed that the adsorption increased slowly until the adsorption reached equilibrium (optimum contact time). Afterwards, there is almost no further increase in the adsorption, therefore, leading to desorption. At this stage, the adsorption diminished which was likely due to less available adsorption sites. A similar trend In addition, the rate of desorption occurred due to slow pore diffusion of the pollutants into the adsorbents and longer diffusion in the inner cavities in exiguous adsorbate (Zou et al., 2019).

3.6.2. *Effect of dosage*

The adsorbent dosage is a paramount parameter responsible for the adsorption of pollutants by the adsorbent. The effect of adsorbent dose on the percentage removal of BOD, COD and nitrate from wastewater are presented in Fig. 8. It was found that the percentage removal efficiency of all pollutants increased with an increase in dosage for both kaolin and kaolin/TiO_2. For instance, the removal efficiency of COD increased from 84.5 to 90.04 and 90.04–92.5 %, BOD from 83.92 to 89.73 and 91.60–94.23 %, nitrate from 84.62 to 92.39 and 88.08–96.56 % for kaolin and kaolin/TiO_2 nanocomposite, respectively (Fig. 9). While the level of Cd removal increased from 45.88 to 75.29 and 52.94–87.06 %, Cr from 41.46 to 87.81 and 43.90–88.62 %, Pb from 54.22 to 72.29 and 61.45–75.90 % for kaolin and kaolin/TiO_2 nanocomposite, respectively (see Fig. 9). It was observed that all parameters followed similar trends. At a lower dosage, the rate of adsorption was influenced by inter ionic competition among the metal ions which is due to the presence of small surface area. The trend in term of heavy metal removal by the two materials was Cr > Cd > Pb. This behavioural pattern can be linked to the difference in the atomic weights and ionic radii of the concern metal ions. At higher dosage, the adsorption process increased due to the availability of more active binding exchangeable sites for adsorption of target pollutants (Abukhadra and Mohamed, 2019). Thus, for every dose of material used, it was found that kaolin/TiO_2 performed better than kaolin alone due to high surface area and

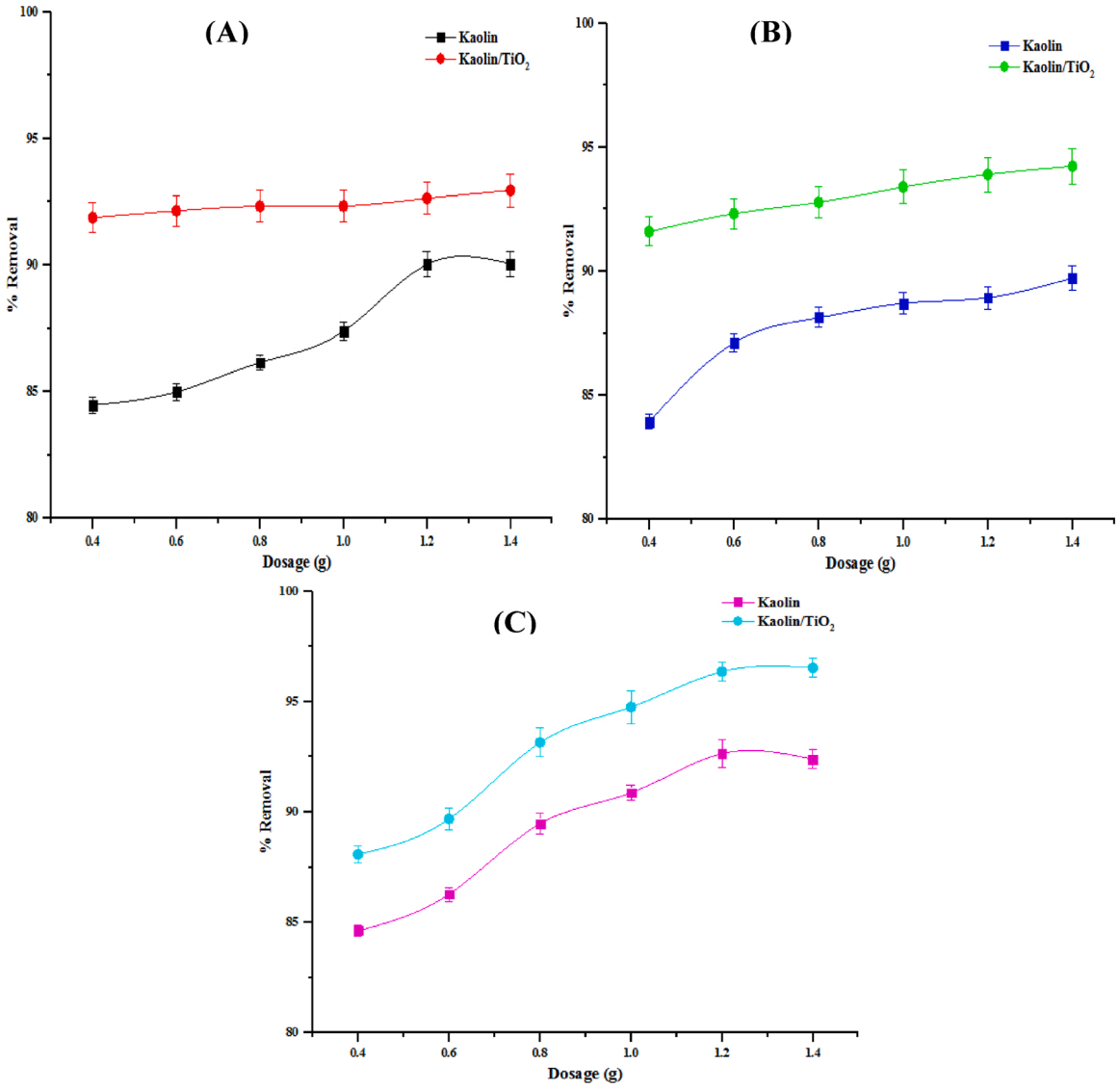

Fig. 8. Effect of adsorbent dosage on percentage removal of (a) COD (b) BOD and (c) nitrate onto beneficiated kaolin and kaolin/TiO_2 nanocomposite (conditions: equilibrium time, agitation speed 150 rpm, temperature 29 °C).

functional groups of the former than the latter. Thus, the pollutants removal efficiency in the tannery wastewater strongly depends on the dosage of the nanoadsorbents.

3.6.3. *Effect of temperature*

The effect of temperature in adsorption studies has a great impact on the adsorption capacity, influenced by the diffusion rate of adsorbate molecules and the internal pores of the adsorbent. Increasing the temperature in an adsorption system brings about an increase in chemical reaction rate (Mekatel et al., 2015). The effects of temperature on the sequestration of COD, BOD, nitrate, Pb, Cd and Cr onto kaolin and kaolin/TiO_2 are shown in Figs. Fig. 1010 and Fig. 1111 . It was generally found that increase in temperature (30−80 °C) corresponds to the increase in the removal efficiencies of the target pollutants and the indicator parameters. The percentage removal of COD, BOD, nitrate, Pb, Cd and Cr increased from 77.43 to 85.34, 75.02–86.31, 51.56–70.58, 26.47–54.12, 58.54–89.43 and 56.02–76.87 % for kaolin, respectively. Similarly, with an increase in temperature, the percentage adsorption of COD, BOD, nitrate, Pb, Cd and Cr showed an increase from 85.46 to 90.29, 83.60 to 89.56, 57.53 to 76.29. 38.24 to 92.15, 51.22 to 91.87 and 62.05 to 78.92 % for kaolin/TiO_2 nanocomposites. From the Figures, an increase in temperature generally increases the percentage removal. The absorptivity and adsorption in the system suggested that sequestration of these pollutants were favoured at high temperature. Interaction among the functional groups present in the nanoadsorbents with the adsorbate led to the formation of strong bonds with an increase in temperature. Kariim et al. (2020) who investigated adsorption of phenol and cyanide using TiO_2/MWCNTs argued that sorption behaviour of TiO_2/MWCNTs was dependent on the surface functional groups of the nanoadsorbent and temperature. Thus, it was demonstrated that the rate of adsorption become faster and endothermic in nature. Comparing the adsorption potential of kaolin and kaolin/TiO_2 for the parameters, it is clear that the adsorption followed the order of kaolin/TiO_2 > kaolin and proved that the addition of TiO_2 nanoparticles improved the adsorption capacity of the nanocomposite.

3.7. *Adsorption isotherms*

3.7.1. *Langmuir isotherm*

Langmuir isotherm assumes the homogeneous adsorption on the surface of adsorbent. The equation of the isotherm is as follows:

$$\frac{C_e}{q_e} = \frac{1}{Q_m K_L} + \frac{1}{Q_m} C_e \quad (5)$$

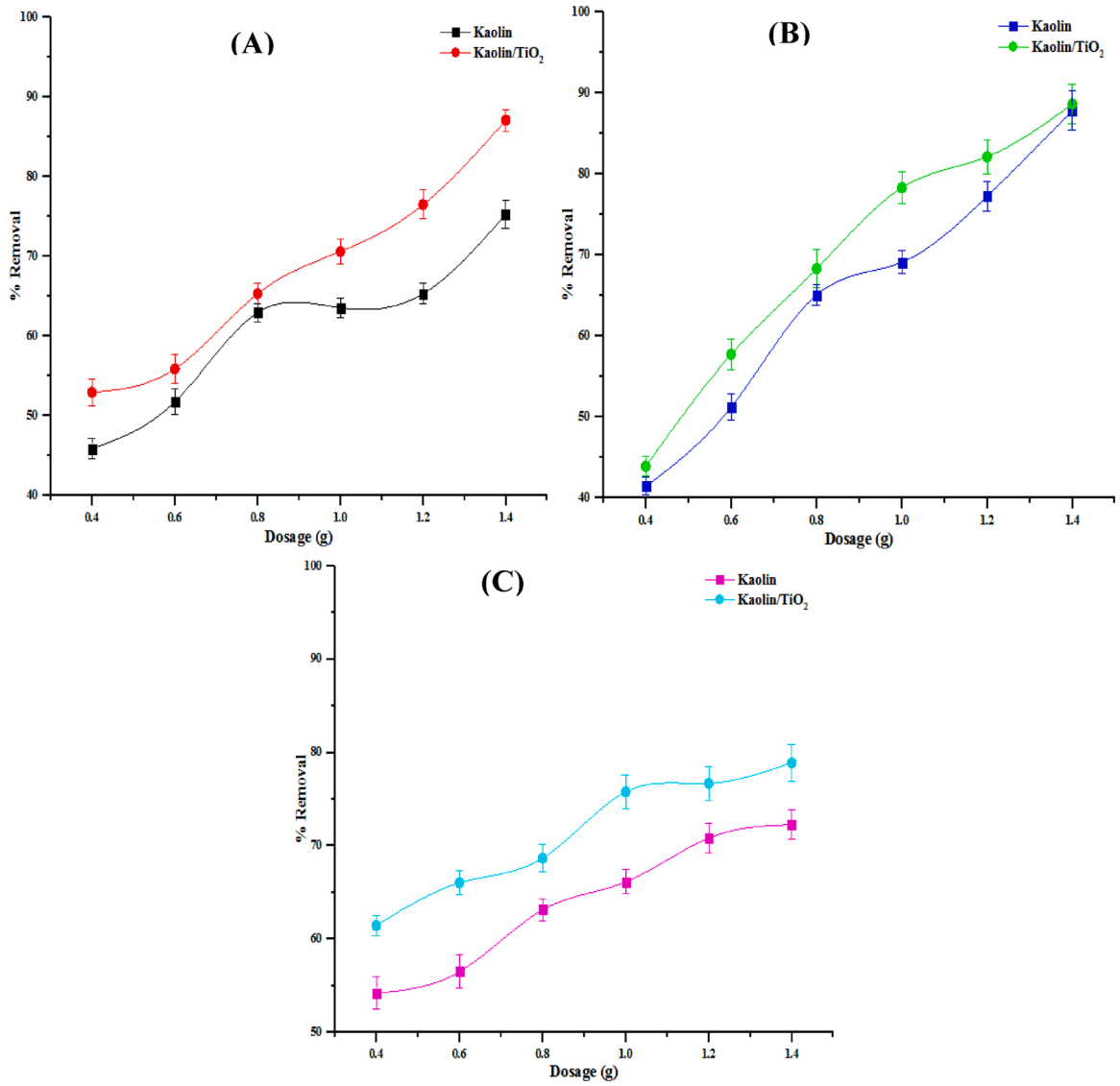

Fig. 9. Effect of adsorbent dosage on percentage removal of (A) Cd (B) Cr and (C) Pb onto beneficiated kaolin and kaolin/TiO_2 nanocomposite (conditions: equilibrium time, agitation speed 150 rpm, temperature 29 °C).

where C_e is the equilibrium concentration of the pollutants in the solution (mg/dm^3), q_e represents the equilibrium adsorption capacity (mg/g), Q_m is the maximum adsorption capacity (mg/g) and K_L denotes Langmuir constant that signifies the affinity between adsorbate and adsorbent (L/mg). The results of Langmuir isotherm constants for COD, BOD, nitrate and selected heavy metals are depicted in Tables 5 and 6, respectively. The maximum adsorption capacity values computed from the Langmuir isotherm indicate the potential application of the adsorbents for tannery wastewater.

3.7.2. Freundlich isotherm

Freundlich isotherms represents multilayer adsorption adsorbent surface and it is given by the Eq. 6.

$$\ln q_e = \frac{1}{n}\ln C_e + \ln K_f \quad (6)$$

where K_f and n are Freundlich constant that are related to adsorption capacity and adsorption intensity, respectively. The results of Freundlich parameters obtained for pollutants removal are given in Tables 5 and 6. The magnitude of the Freundlich constant, n, shows a favourable adsorption. It is generally described that value of n between 2 and 10 indicates good adsorption features (Khayyun and Mseer, 2019). This implies that the studied adsorbents (kaolin and kaolin/TiO_2) are good for removal of pollutants from wastewater.

3.7.3. Halsey isotherm

Halsey model (1948) was employed to evaluate the multilayer adsorption at a relatively large distance from the surface of the adsorbents. The equation of the Halsey isotherm is given as follows:

$$q_e = \frac{1}{n_H} I_n K_H - \frac{1}{n_H}\ln C_e \quad (7)$$

where n_H and I_nK_H are Halsey isotherm constants and these were determined from the slope and intercept of the linear plot of q_e as the ordinate and $\ln C_e$ as the abscissa at the temperature range of 30–80 °C, constant pH 5.84 and adsorbent dosage of 0.2 g.

Tables 5 and 6 show Halsey model isotherm constants (n_H and I_nK_H) for the removal of physicochemical parameters in tannery wastewater. The model is selected due to the multilayer adsorption and the fitting to the nature of kaolin and nanocomposite materials. It is evident that the linear correlation coefficient (R^2) for kaolin and nanocomposites in the removal of physicochemical parameters such as BOD, COD, nitrate, Pb,

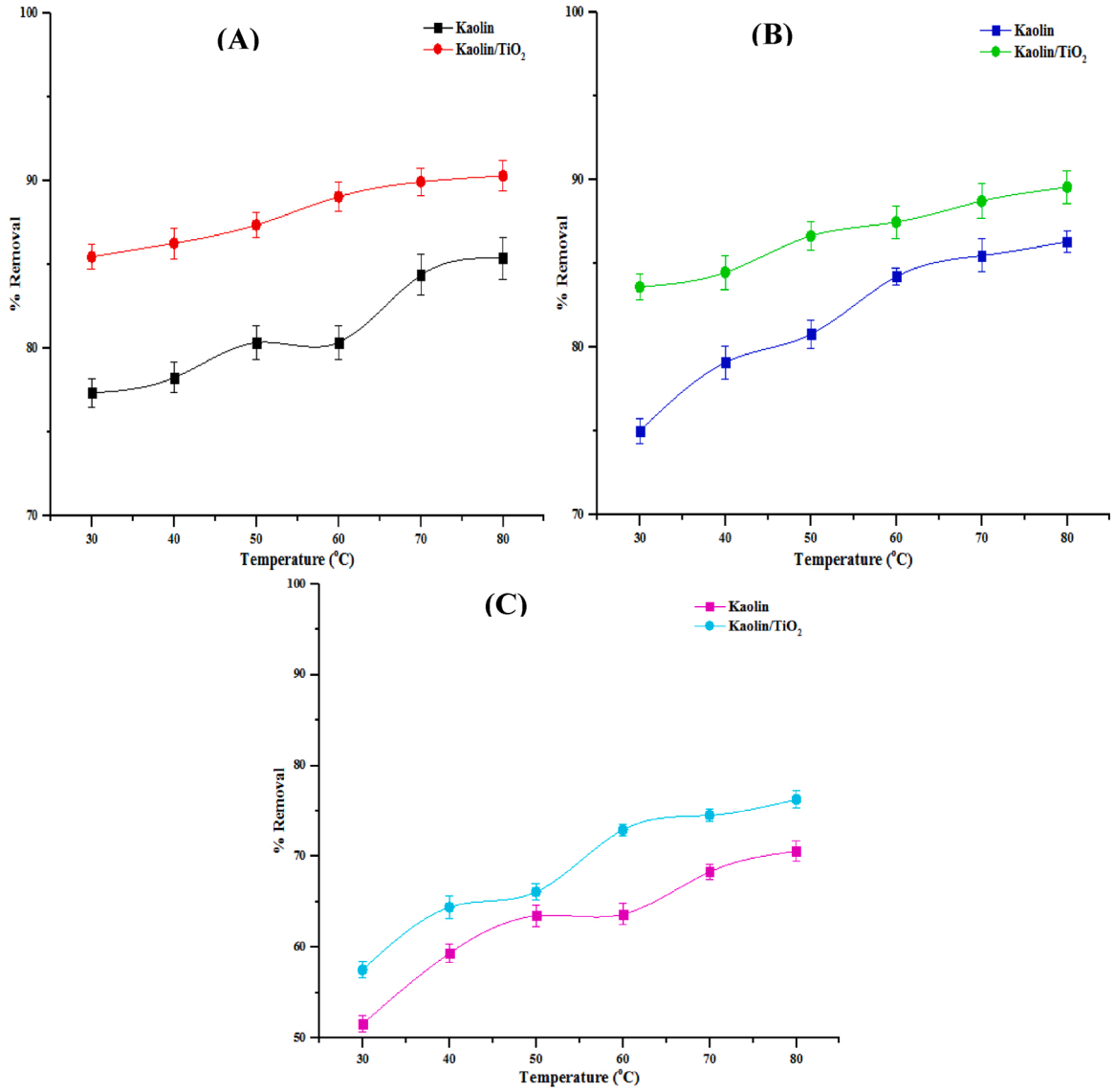

Fig. 10. Effect of temperature on percentage removal of (A) COD (B) BOD and (C) nitrate onto beneficiated kaolin and kaolin/TiO_2 nanocomposite (conditions: adsorbent dose 0.2 g, agitation speed 150 rpm).

Cd and Cr is > 0.98. This shows that the experimental data moderately fit Halsey and the adsorption of these pollutants onto the adsorbent materials could partially be based on multilayer adsorption.

3.7.4. Jovanovic isotherm

Jovanovic model (1969) was based on the assumption of the Langmuir model and the possibility of some mechanical contacts between the sorbate and adsorbents. The linear form of the model is given as follows:

$$\ln q_e = \ln q_{e(max)} - K_j C_e \quad (8)$$

A plot of $\ln q_e$ against C_e enables the determination of Jovanovic constant (K_j) and the maximum adsorption capacity ($q_{e(max)}$), where K_j, is the slope and $q_{e(max)}$ is the intercept. The values of Jovanovic constant (K_j) and maximum adsorption capacity ($q_{e(max)}$) for this adsorption system and the experimental information were provided in Tables 5 and 6. It is apparent that the correlation coefficient is > 0.99 and this confirmed that the experimental data on the removal of the target pollutants by kaolin and kaolin/TiO_2 fitted well for the isotherm model. It also showed that (R^2) values of Jovanovic isotherm model were higher than Halsey model which indicates the occurrence of some mechanical contacts between the adsorbate (tannery wastewater) and adsorbent (nanoadsorbents) phase interface. The adsorption surface also considered the system to be homogeneous with monolayer localized adsorption similar to that Langmuir model which could be as a result of the presence of some functional groups from kaolin and kaolin/TiO_2 nanoadsorbents. The maximum adsorption capacity values obtained for the uptake of metal ions using kaolin/TiO_2 nanoadsorbent were compared to those of some adsorbents reported in literature in Table 7.

3.7.5. Redlich-Peterson (R-P) isotherm

The Redlich-Peterson (R-P) isotherm (1959) is the combination of the Langmuir and Freundlich adsorption models and can be linearized as follows:

$$\ln \frac{C_e}{q_e} = \beta \ln C_e - \ln A \quad (9)$$

where the isotherm constants β and A are determined from the slope and intercept of a plot of $\ln \frac{C_e}{q_e}$ as the abscissa and $\ln C_e$ as the ordinate, respectively. The Redlich-Peterson model provides information on the isotherm constants β and A from the slopes and intercepts. The value of A presented in Tables 5 and 6 show that the adsorption capacity of the

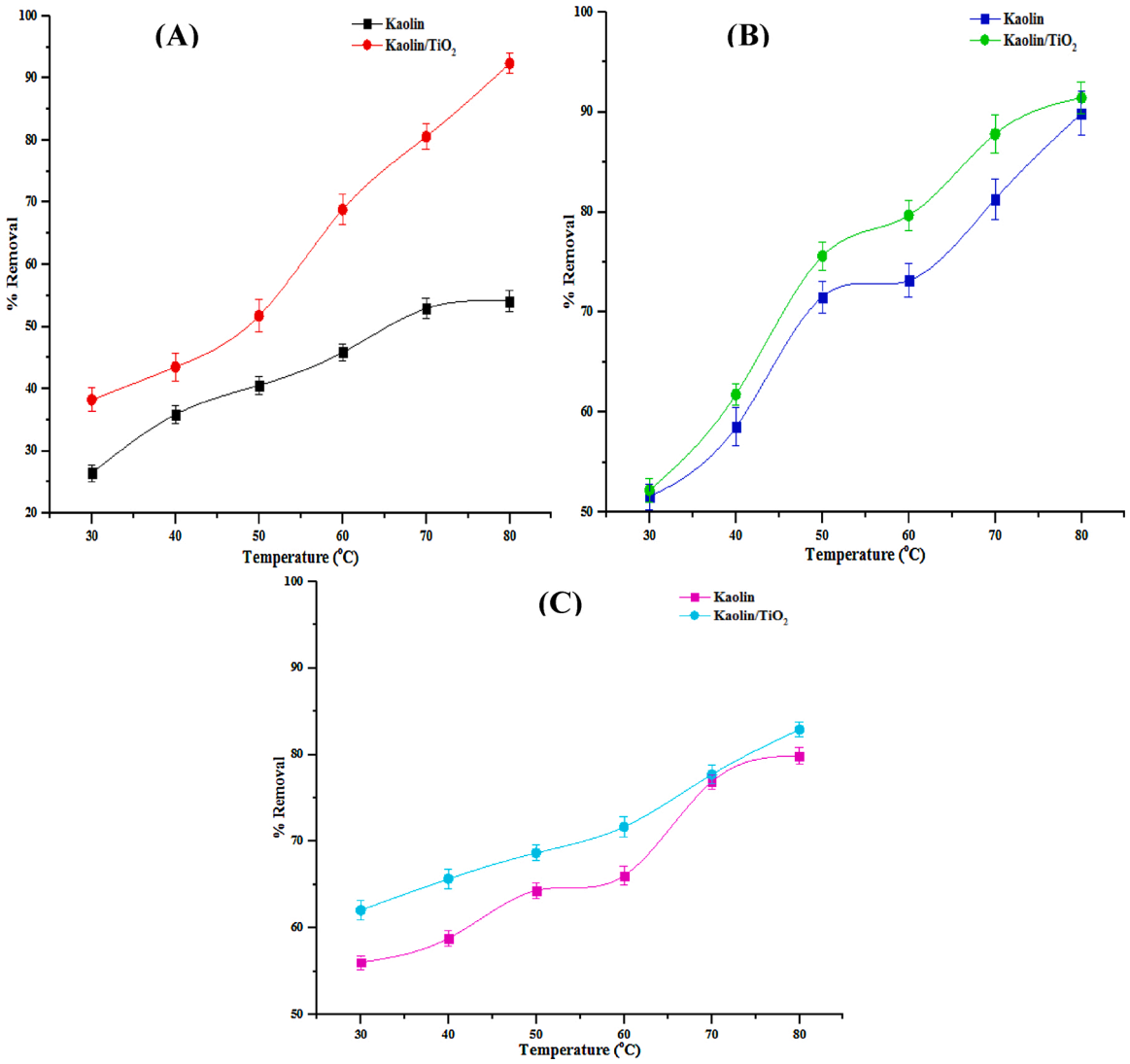

Fig. 11. Effect of temperature on percentage removal of (A) Pb (C) Cd and (C) Cr onto beneficiated kaolin and kaolin/TiO_2 nanocomposite (conditions: adsorbent dose 0.2 g, agitation speed 150 rpm).

adsorbents was higher in kaolin/TiO_2 than kaolin nanoparticles and the value of β were slightly above 1 for the pollutant uptake onto the adsorbents. The Redlich-Peterson isotherm described three parameters empirical adsorption parameters model and improve both the Langmuir and Freundlich equation. In this study, Langmuir isotherm was more appreciated than the Freundlich model. The experimental data for the R-P isotherm followed the adsorption of the pollutants uptake in wastewater with corresponding correlation coefficient ($R^2 > 0.999$) as shown in Tables . The R^2 values show the good fitting of the experimental data to the R-P adsorption model.

3.7.6. *Flory-Huggins isotherm*

The Flory-Huggins isotherm model (1956) evaluates the degree of surface coverage properties of the sorbate on the sorbent. The Flory-Huggins model is defined by the following expression:

$$\ln\frac{\theta}{C_o} = \ln K_{FH} + n\ln(1-\theta) \tag{10}$$

$$\theta = (1-\frac{C_e}{C_o}) \tag{11}$$

The adsorption data at different temperature were plotted as a function of $\ln\frac{\theta}{C_o}$ against $\ln(1-\theta)$. Where n is the number of adsorbates occupying adsorption site, θ is the degree of surface coverage and K_{FH} is the Flory-Hugging constants.

The linear form of the Flory-Huggins isotherm model displayed the Flory-Huggins equilibrium constant (K_{FH}) as presented in Tables 5 and 6. The isotherm model expressed the feasibility and spontaneity of the adsorption process. The evaluated K_{FH} used to calculate the spontaneity Gibb's free energy (ΔG) showed that the value is negative. This indicates the influence of temperature during the adsorption system. Thus, the adsorptivity is temperature-dependent. Conversely, the obtained R^2 value for this isotherm model is related to that of Halsey isotherm.

From the different isotherms employed in this study, the values of their correlation coefficient, sum of square error (SSE) and Chi- square (χ^2) of polltants are shown in Tables 5 and 6. The lowest values of SSE and χ^2 for the isotherms suggest the applicability of the model to the adsorption of the studied pollutants onto kaolin and kaolin/TiO_2 nanocomposites. It was observed that low sum of square error and Chi square values for the isotherm model best described the adsorption of pollutants onto the adsorbents. Thus, the Redlich- Peterson model with lowest value of error parameter best described the removal of pollutants except for Pb ion compared to other models in this study.

Table 5
The parameters of adsorption isotherms of BOD, COD and nitrate removal using kaolin and kaolin/TiO_2 (KT) at dosage (0.2 g) and pH (5.84).

Isotherm	Parameter	COD		BOD		Nitrate	
		Kaolin	KT	Kaolin	KT	Kaolin	KT
Langmuir	Q_m	289.474	303.030	81.301	93.458	117.371	135.506
	K_L	0.0137	0.0358	0.0454	0.0906	0.0474	0.0591
	R^2	0.99930	0.99980	0.99840	0.99970	0.98990	0.99330
	SSE	5.412	4.143	4.770	2.516	6.115	6.019
	χ^2	0.244	0.233	0.138	0.130	0.308	0.286
Freundlich	K_f	121.100	73.320	30.011	65.270	15.640	8.885
	n	4.474	7.386	4.359	6.527	1.573	2.108
	R^2	0.99550	0.99700	0.98930	0.99630	0.98260	0.98580
	SSE	6.405	4.216	5.628	3.930	7.481	8.205
	χ^2	0.495	0.248	0.257	0.245	0.462	0.401
Jovanovic	q_{max}	401.015	406.669	110.469	127.996	125.834	147.322
	K_j	6.175	5.720	1.980	1.850	1.396	1.264
	R^2	0.99979	0.99995	0.99949	0.99992	0.99679	0.99795
	SSE	4.812	4.072	4.630	2.318	5.067	5.361
	χ^2	0.226	0.211	0.135	0.0983	0.194	0.267
Halsey	n_H	4.474	7.386	4.360	6.528	1.598	2.108
	I_nK_H	31.756	48.726	24.885	34.996	8.076	9.458
	R^2	0.99434	0.99627	0.98658	0.99532	0.99824	0.98224
	SSE	8.108	4.470	5.035	4.584	4.705	9.109
	χ^2	0.574	0.251	0.323	0.281	0.134	0.644
Flory-H	n	−0.224	−0.135	−0.229	−0.153	−0.626	−0.424
	K_{FH}	2.800×10^{-4}	3.315×10^{-4}	8.793×10^{-4}	1.015×10^{-3}	2.820×10^{-3}	3.297×10^{-3}
	R^2	0.99434	0.99627	0.98658	0.90000	0.97824	0.98224
	SSE	8.272	4.481	5.060	6.920	8.706	9.251
	χ^2	0.575	0.225	0.341	0.4825	0.503	0.648
Redlich-P	β	1.224	1.135	1.229	1.153	1.626	1.474
	A	1.210×10^3	7.332×10^2	3.011×10^2	2.129×10^2	1.564×10^2	8.885×10^1
	R^2	0.99981	0.99995	0.99953	0.99992	0.99673	0.99814
	SSE	4.617	4.070	4.140	2.337	4.982	5.253
	χ^2	0.215	0.221	0.122	0.105	0.172	0.248

3.8. Kinetic models

The adsorption mechanism, as well as rate controlling steps during the adsorption of the studied pollutants by the nanoadsorbent with respect to contact time (0−30 min), can be established using kinetic models.

3.8.1. Pseudo-first order model and pseudo-second order model

The pseudo-first order kinetic model assumes that the rate of sorption is proportional to the active adsorbent sites. The equation of Lagergren pseudo-first order is given by Eq. (.12.)

$$\ln(q_e - q_t) = \ln q_e - k_1 t \tag{12}$$

where q_e and q_t denote the amount of pollutant adsorbed (mg/g) at equilibrium and at time, t, respectively and k_1 is the rate constant of pseudo-first order adsorption (min^{-1}). The values of q_e, k_1 and R^2, for the pollutant removal using kaolin and kaolin/TiO_2 are presented in Tables 8 and 9.

The pseudo-second order assumes that rate of adsorption sites is proportional to the square of the number of unoccupied adsorbent sites. The equation of pseudo-second order is describe as follows;

$$\frac{t}{q_t} = \frac{1}{k_2 q_e^2} + \frac{t}{q_e} \tag{13}$$

where q_e and q_t are the amount of pollutant adsorbed at equilibrium and at time, t, respectively and k_2 is the rate constant of pseudo-second order adsorption kinetic (g/mg/min). As seen in Tables 8 and 9, the results show that the pseudo-second order kinetic model is more applicable to describe the adsorption kinetics of pollutants onto kaolin and kaolin/TiO_2 than other models. The calculated k_2 value was found to be highest for Cr ion followed by Cd and Pb ion, which was based on the ionic radius mechanism of the adsorbed metal ions. This indicated that the less the hydrated ionic radius, the high is the pseudo-second order rate constant value.

3.8.2. Other kinetic models

The data obtained were analysed using the Bangham, fractional power and Avrami equation models. The Boyd kinetic equation and Weber-Morris intra-particle diffusion models were used to check the mechanism of adsorption.

Bangham's model equation is expressed as:

$$\log\left[\log\left(\frac{C_o}{C_o - q_t M}\right)\right] = \log\left(\frac{K_o M}{2.303V}\right) + \alpha \log t \tag{14}$$

where C_o is the initial concentration of the pollutant in wastewater solution (mg/dm^3), V is the volume of wastewater solution (dm^3), M is the weight of adsorbent (g/dm^3) qt is the amount of pollutant adsorbed at the time, t (mg/g) and K_o and α (less than 1) are constant which are calculated from the intercept and slope of the linear plot of $\log\left[\log\left(\frac{C_o}{C_o - q_t M}\right)\right]$ against logt.

The Bangham kinetic model explained the pore diffusion between the adsorbate and adsorbent in the adsorption system and the α and Bangham constants (see Tables 8 and 9). The extrapolation of the double logarithm order kinetic model showed that multiple adsorption stages occurred and the correlation coefficient (R^2) obtained for the model range between 0.6421 and 0.99248, suggest that pore diffusion was involved in the pollutants removal using kaolin and kaolin/TiO_2. On the other hand, the linearity of the Bangham plot indicates that the sorbate pore diffusion is not the solitary rate controlling step.

The Avrami equation was used to evaluate the kinetic parameter as a

Table 6
The parameters of adsorption isotherms of Pb, Cd and Cr removal using kaolin and kaolin/TiO_2 (KT) at dosage (0.2 g) and pH (5.84).

Isotherm	Parameter	Pb		Cd		Cr	
		Kaolin	KT	Kaolin	KT	Kaolin	KT
Langmuir	Q_m	24.307	26.460	22.883	28.035	73.529	83.057
	K_L	0.0249	0.0288	0.0383	0.0470	0.118	0.150
	R^2	0.98360	0.98170	0.96150	0.96450	0.99210	0.99540
	SSE	221.02	227.536	185.204	172.120	160.948	157.525
	χ^2	4.233	9.349	8.840	6.822	6.716	6.321
Freundlich	K_f	17.46	16.45	9.759	8.282	17.458	16.448
	n	2.129	2.535	2.425	3.300	2.129	2.535
	R^2	0.98420	0.98880	0.86480	0.89760	0.98420	0.98880
	SSE	203.18	180.364	190.47	189.370	167.003	162.356
	χ^2	4.019	6.102	10.583	8.562	7.815	7.064
Jovanovic	q_{max}	53.524	66.341	72.257	87.260	107.678	128.094
	K_j	1.553	0.955	1.129	1.166	0.170	0.1804
	R^2	0.99085	0.98481	0.98540	0.99671	0.99861	0.99760
	SSE	200.035	213.20	172.508	160.206	150.422	152.001
	χ^2	3.150	8.020	7.326	6.314	5.683	5.925
Halsey	n_H	0.642	2.446	3.155	3.300	2.129	2.535
	I_nK_H	0.170	1.059	−6.694	−6.998	4.258	7.098
	R^2	0.97315	0.83163	0.83106	0.93381	0.98028	0.98596
	SSE	241.10	231.903	191.950	180.403	172.834	165.140
	χ^2	4.860	9.734	10.835	7.654	8.021	8.302
Flory-H	n	−1.558	−0.409	−0.317	−0.303	−0.470	−0.395
	K_{FH}	9.865×10^{-2}	2.147×10^{-1}	3.709×10^{-1}	3.748×10^{-1}	4.689×10^{-2}	5.180×10^{-2}
	R^2	0.97315	0.83163	0.93106	0.93381	0.98028	0.98596
	SSE	241.52	232.081	186.211	181.320	172.901	165.230
	χ^2	4.902	9.800	8.922	7.812	8.392	8.472
Redlich-P	β	2.558	1.409	1.317	1.303	1.395	1.470
	A	1.303	1.542	0.120	0.121	16.450	17.460
	R^2	0.98990	0.98383	0.99596	0.98953	0.99796	0.99886
	SSE	197.30	221.603	160.341	168.910	153.741	150.603
	χ^2	3.018	9.034	6.719	6.520	5.935	5.417

Table 7
Comparative study of maximum adsorption capacity for Pb, Cd and Cr ion reported in different literature.

Adsorbent	Metal ion	Q_m (mg/g)	Reference
Montmorillonite	Pb and Cr	21.46 and 18.08	Barbooti (2015)
Natural clay	Pb	25.07	Kushwaha et al. (2020)
Clay/TiO_2	Cd	8.92	Sharififard et al. (2018)
Bentonite	Cd	8.20	Burham and Sayed (2016)
Chitosan/clay	Cr	80.30	Foroutan et al. (2020)
Sludge/TiO_2	Cd	29.28	Sharaf El-Deen and Zhang (2016)
Kaolin	Cr	15.82	Deng et al. (2014)
Amino modified clay	Cr	36.91	Li et al. (2019)
Ball clay	Cd	27.17	Rao and Kashifuddin (2016)
Kaolinite/smectite	Pb	0.78	El-Naggar et al. (2019)
Kaolin/TiO_2	Pb	*26.46 **66.34	This work
Kaolin/TiO_2	Cd	*28.06 **87.26	This work
Kaolin/TiO_2	Cr	*83.06 **128.09	This work

Key: * = Langmuir; ** = Jovanovic.

function of the contact time (0−30 min). The linear form of the Avrami kinetic model is expressed as:

$$\ln\left[\ln\left(\frac{q_e}{q_e - q_t}\right)\right] = n_{AV}\ln K_{AV} + n_{AV}\ln t \quad (15)$$

where K_{AV} is the Avrami kinetic constant and n_{AV} is the Avrami model constant related to the adsorption mechanism. The values of K_{AV} and n_{AV} are obtained for the intercept and slope, respectively, from the plot of $\ln\left[\ln\left(\frac{q_e}{q_e - q_t}\right)\right]$ versus lnt.

The Avrami kinetic parameters rate constant (K_{AV}), Avrami exponent (A_{AV}) and correlation coefficient (R^2) are presented in Tables 8 and 9. The A_{AV} values were positive in all the pollutants uptake onto the adsorbents. This shows that there was contact between the adsorbate with the adsorbents and the rate of adsorption favoured multiple kinetic orders. The kinetic data suitably fitted well to the Avrami kinetic model due to its highest R^2 values for all the studied pollutants using kaolin and kaolin/TiO_2 nanocomposites compared to Bangham and fractional power kinetic models. Equ. 10 depicted the linear form of power model represented as follows:

$$\log q_t = \log K + V\log t \quad (16)$$

where V and K are constants with V less than 1. The values of V and K are slope and intercept obtained from the plot of $\log q_t$ against logt, respectively. The fitness of the kinetic models to the experimental data in this study were determined using Chi square error analysis. The kinetic parameters and their respective error functions were shown in Tables 8 and 9. The model with the least values for the error parameter and the highest R^2 value indicates the best kinetic of pollutant adsorption.

3.9. Mechanism of adsorption

The adsorption mechanism of the pollutant removal using kaolin and kaolin/TiO_2, nanocomposites were investigated using Weber-Morris intra-particle diffusion and Boyd models. The Weber-Morris equation proposed for modelling adsorption kinetic is expressed as:

Table 8
The parameters of kinetic models of COD, BOD and nitrate removal using kaolin and kaolin/TiO_2 (KT) at dosage (0.2 g), temperature (298 K) and pH (5.84).

Kinetic	Parameter	COD		BOD		Nitrate	
		Kaolin	KT	Kaolin	KT	Kaolin	KT
Pseudo-first	q_e	122.570	147.540	140.851	360.864	7.447	14.556
	k_1	4.70×10^{-3}	7.40×10^{-3}	3.70×10^{-3}	6.9×10^{-3}	1.10×10^{-3}	2.61×10^{-3}
	R^2	0.71150	0.90245	0.82170	0.89410	0.92100	0.93680
	χ^2	13.164	9.646	10.618	5.672	6.140	5.630
Pseudo-second	q_e	294.118	370.170	102.041	114.943	12.788	21.505
	k_2	1.204×10^{-3}	3.645×10^{-3}	3.201×10^{-2}	4.569×10^{-2}	1.26×10^{-2}	4.805×10^{-2}
	R^2	0.88720	0.99990	0.99870	0.99999	0.99720	0.99990
	χ^2	9.201	6.516	9.810	3.743	4.002	3.405
Fractional-P	K	242.103	302.691	85.198	103.455	12.159	18.059
	V	0.052	0.065	0.0534	0.0363	0.0409	0.0588
	KV	12.589	19.675	4.550	3.755	0.497	1.062
	R^2	0.75652	0.90404	0.74321	0.88001	0.75352	0.86739
	χ^2	12.360	8.624	13.201	8.504	8.961	6.001
Bangham	α	0.0529	0.0633	0.0543	0.0358	0.0680	0.0598
	K_i	4.935	6.244	5.527	6.750	3.852	6.203
	R^2	0.6542	0.90401	0.68402	0.88789	0.86760	0.94218
	χ^2	15.406	8.269	14.606	7.310	7.823	5.218
Avrami	n_{AV}	0.2292	0.470	0.272	0.305	0.417	0.414
	K_{AV}	−0.119	2.216	1.597	4.896	−1.919	2.397
	R^2	0.80454	0.90502	0.76954	0.87159	0.92549	0.95326
	χ^2	10.503	7.366	12.944	8.900	5.361	4.728

Table 9
The parameters of kinetic models of Pb, Cd and Cr removal using kaolin and kaolin/TiO_2 (KT) at dosage (0.2 g), temperature (298 K) and pH (5.84).

Kinetic	Parameter	Pb		Cd		Cr	
		Kaolin	KT	Kaolin	KT	Kaolin	KT
Pseudo-first	q_e	2.056	2.392	1.074	2.480	6.441	8.311
	k_1	5.10×10^{-2}	8.32×10^{-2}	5.44×10^{-2}	9.64×10^{-2}	5.12×10^{-2}	8.57×10^{-2}
	R^2	0.60810	0.71200	0.47760	0.59320	0.84210	0.89190
	χ^2	16.412	13.225	20.914	20.588	13.972	11.513
Pseudo-second	q_e	6..988	7.121	2.012	4.067	8.269	10.376
	k_2	1.70×10^{-3}	3.25×10^{-3}	1.18×10^{-2}	1.98×10^{-2}	1.67×10^{-1}	2.21×10^{-1}
	R^2	0.87560	0.92380	0.86990	0.90900	0.99170	0.99790
	χ^2	13.182	11.305	17.143	15.648	10.816	9.017
Fractional-P	K	0.125	0.134	0.0783	0.0868	0.797	0.881
	V	0.153	0.1471	0.2319	0.1903	0.02132	0.0508
	KV	0.0191	0.0197	0.0182	0.0165	0.0169	0.0445
	R^2	0.76292	0.80156	0.58217	0.85008	071,921	0.81364
	χ^2	15.912	12.910	19.771	16.052	15.401	13.267
Bangham	α	0.155	0.149	0.234	0.205	0.025	0.0514
	K_i	2.962	3.185	2.563	2.762	3.877	4.292
	R^2	0.76265	0.80144	0.68486	0.84886	0.71904	0.81352
	χ^2	15.860	12.855	19.026	16.514	15.649	13.552
Avrami	n_{AV}	0.381	0.424	0.863	0.684	0.520	0.591
	K_{AV}	−2.535	−2.551	−1.981	−2.157	−2.165	−1.332
	R^2	0.85199	0.91171	0.77477	0.77294	0.84700	0.89200
	χ^2	14.520	11.940	18.104	17.991	13.759	11.243

$$q_t = K_d t^{1/2} + I \quad (17)$$

Where K_d ($mg^{-1}\ min^{-1/2}$) is the intraparticle diffusion rate constant, I is a constant that shows the thickness of boundary i.e the greater the intercept, the greater the rate-controlling step on the adsorption surface. The I and K_d are the intercept and slope, respectively, which are evaluated from the linear plot of q_t against $t^{1/2}$.

Boyd model was used to analyse the rate-controlling step in the adsorption of the studied pollutants by kaolin and kaolin/TiO_2 nanocomposites. The Boyd kinetic equation is presented as:

$$F = 1 - \frac{6}{\pi}\exp(-B_t) \quad (18)$$

$$F = \frac{q_t}{q_e} \quad (19)$$

Where q_t and q_e in (mg/g) are the amounts of adsorbate uptake at the time and maximum equilibrium uptake. F is the fraction of pollutant adsorbed at any time, t.

$$B_t = -0.4977 - \ln(1 - F) \quad (20)$$

B_t is the time constant and is a function of F. The linear plot of B_t against time, t is employed for the experimental data.

The Boyd and intra-particle diffusion models suggest the occurrence of some degree of boundary layer diffusion during the removal of the studied pollutant by the adsorbents. The intercept, (I) values are > 0 for all the pollutants while Tables 10a and 10b indicate that the intra-particle diffusion was not the only controlling step. The result obtained implies that the rate of adsorption of the pollutants involved multi-kinetic stages. Also, the Boyd kinetic helps to identify whether the rate-determining step is an external transport or intra-particle transport during the adsorption process. The linearity indicates that the initial concentration of the pollutants and external mass transport controlled the rate of adsorption.

Considering the intraparticle diffusion and Boyd models, the mechanism for the studied pollutants uptake onto the adsorbents may follow these assumptions: (i) bulk diffusion (ii) film diffusion (iii) intraparticle or pore diffusion (iv) ionic nature of the sorbate (chemical reaction through ion exchange).

3.10. Thermodynamic studies

In order to understand the mechanism involved in the adsorption process vis-a-viz effect of temperature; thermodynamic parameters were studied and evaluated from the adsorption system. The change in Gibbs free energy (ΔG), enthalpy (ΔH) and entropy (ΔS) at respective temperatures were computed using the following equations:

$$K_d = \frac{q_e}{C_e} \tag{21}$$

$$\Delta G = -RT\ln K_d \tag{22}$$

$$\Delta G = \Delta H - T\Delta S \tag{23}$$

Where the values of ΔG, ΔH and ΔS were measured in kJ/mol, kJ/mol and J/molK respectively. T is the absolute temperature (K), R is the universal gas constant (8.314 J/molK). The ΔH and ΔS were evaluated from the slope and the intercept through the extrapolation from the plot of distribution coefficient (K) against $\frac{1}{T}$. The values of ΔH, ΔS and ΔG are presented in Tables 11 and 12.

According to Tables 11 and 12, it can be observed that the value of ΔH and ΔS were positive. The positive value of ΔH showed that the adsorption process was endothermic in nature. While the positive value of ΔS indicated an increase in the degree of randomness during the sorbate-sorbent interaction. Taghlidabad et al. (2020) reported similar finding on the adsorption of Cd ion using biochar as an adsorbent. They noticed that the adsorption of Cd ion increased with an increasing temperature. However, in this case, it was observed that the Gibbs free energy-reduced with an increase in temperature indicating driving force, leading to higher adsorption capacity. Therefore, at higher temperature, adsorption process increased owing to the increase in randomness of adsorbent-adsorbate interface. The thermodynamic studies on the removal of these pollutants suggest chemical adsorption (chemical bonds) due to the strong interface between the adsorbate and adsorbents, allowing pollutant to adhere on the surface of the nanoadsorbents.

Table 10a
Parameters and correlation coefficient (R^2) of kinetic models for the adsorption of COD, BOD and nitrate onto kaolin/TiO_2.

Parameter	Sample	Boyd Model	Intra-Particle Model		
		R^2	K_{id}	I	R^2
COD	Kaolin	0.81404	7.289	248.713	0.5551
	KT	0.87696	12.578	310.506	0.6427
BOD	Kaolin	0.71006	3.022	86.166	0.66822
	KT	0.87405	2.288	104.746	0.60812
Nitrate	Kaolin	0.75083	0.05834	13.183	0.17301
	KT	0.92246	0.68693	18.367	0.76476

Table 10b
Parameters and correlation coefficient (R^2) of kinetic models for the adsorption of Pb, Cd and Cr onto kaolin/TiO_2 at dosage (0.2 g), temperature (298 K) and pH (5.84).

Parameter	Sample	Boyd Model	Intra-Particle Model		
		R^2	K_{id}	I	R^2
Lead	Kaolin	0.82982	0.0107	0.144	0.21096
	KT	0.90455	0.0152	0.139	0.53946
Cadmium	Kaolin	0.8066	0.0197	0.0709	0.80749
	KT	0.90916	0.0184	0.0761	0.67984
Chromium	Kaolin	0.77958	0.0268	0.846	0.15207
	KT	0.83948	0.0177	0.932	0.72089

3.11. Desorption and regeneration studies

Desorption study of kaolin/TiO_2 nanocomposites is shown in Fig. 12 (a). From the batch elution results, it is evident that the CH_3COOH and deionized water performed poorly as eluting agent. Desorption efficiency in the system follows the order HNO_3 > CH_3COOH > deionized water. Desorption efficiency obtained for kaolin/TiO_2 nanoadsorbents were 98.2 % (Cr), 90.1 % (Cd) and 93 % (Pb) for HNO_3, 67.4 % (Cr), 58.2 % (Cd) and 52.5 % (Pb) for CH_3COOH and 46.9 % (Cr), 54.2 % (Cd) and 51.5 % (Pb) for deionized water. Fig. 12 (b) show the removal efficiency of kaolin/TiO_2 nanoadsorbent cycle when adsorbents were treated with 0.1 M EDTA. The reduction in efficiency of the nanoadsorbents was observed for adsorption of metal ions without regeneration as seen in Fig. 12 (c). In Fig. 12 (b), EDTA showed good desorption ability for regeneration studies for high adsorption tendency of metal ion removal even after the fifth reusability cycles and support the findings of (Wang et al., 2019).

4. Conclusion

In summary, the synthesis, characterization and application of kaolin and kaolin/TiO_2 nanoadsorbents for the removal of toxic pollutants in tannery wastewater were investigated. The synthesized nanoadsorbents were characterized before the adsorption for the removal of COD, BOD, nitrate, cadmium, lead and zinc from tannery wastewater using XRD, FTIR, HRTEM, SAED, EDX, HRSEM and BET. Adsorption studies were performed under different condition such as contact time, dosage and temperature. The kinetic and isotherm studies were used to describe the adsorption equilibrium of the pollutants onto the adsorbents. Sequel to this information, the following conclusions are drawn:

- The characterization result revealed plate-like morphology of the beneficiated kaolin and anatase phase of the synthesized TiO_2 at a calcination temperature of 450 °C.
- XRD, HRSEM, HRTEM, FTIR, EDX and BET demonstrated the presence of the TiO_2 nanoparticles on the layer of kaolin. The nanoadsorbent showed the existence of functional groups related to both kaolinites and TiO_2, and mesoporosity of the adsorbents.
- The optimum conditions for maximum removal of COD, BOD, nitrate, lead, cadmium and chromium adsorption were 0.2 g of the adsorbent, pH 5.84 with 150 rpm shaking speed.
- The adsorption process was greatly dependent on dosage and temperature. The percentage of pollutants removal increased by increasing the dose and temperature. The increase in dosage is due to the increase in the available active sites for the uptake of the pollutants.
- The adsorption data of pollutants fitted best for R-P isotherm model in most cases. Hence, the surface adsorption can be considered as homogeneous with monolayer coverage and high maximum

Table 11
Thermodynamic parameters of COD, BOD and nitrate removal onto kaolin and kaolin/TiO_2 (KT).

Parameter	Sample				ΔG (kJ/mol)					
		R^2	ΔH (kJ/mol)	ΔS (J/molK)	303K	313K	323K	333K	343K	353K
COD	Kaolin	0.88560	9.827	28.816	1.096	0.808	−0.519	0.231	0.569	−0.345
	KT	0.97060	8.923	30.604	−0.350	−0.656	−0.962	−1.268	−1.574	−0.345
BOD	Kaolin	0.97300	13.47	40.48	1.205	0.800	0.395	0.00984	−0.415	−0.819
	KT	0.95646	9.891	32.716	0.022	−0.349	−0.676	−1.003	−1.331	−1.658
Nitrate	Kaolin	0.96578	13.398	32.007	3.700	3.380	3.060	2.740	2.420	2.100
	KT	0.94717	15.562	40.847	3.185	2.777	2.368	1.960	1.552	1.143

Table 12
Thermodynamic parameters of Pb, Cd and Cr removal onto kaolin and kaolin/TiO_2 (KT).

Parameter	Sample				ΔG (kJ/mol)					
		R^2	ΔH (kJ/mol)	ΔS (J/molK)	303K	313K	323K	333K	343K	353K
Lead	Kaolin	0.90400	24.631	77.825	1.053	0.272	−0.507	−1.285	−2.063	−2.841
	KT	0.90121	51.799	169.714	0.376	−1.322	−3.019	−4.716	−6.413	−8.110
Cadmium	Kaolin	0.93850	35.713	105.904	3.624	2.588	1.506	0.447	−0.612	−0.1671
	KT	0.89801	37.629	110.452	4.162	3.058	1.953	0.849	−0.256	−1.361
Chromium	Kaolin	0.90041	18.725	68.898	−2.151	−2.840	−3.529	−4.218	−4.907	−5.596
	KT	0.87628	14.996	58.92	−2.857	−3.446	−4.035	−4.624	−5.214	−5.803

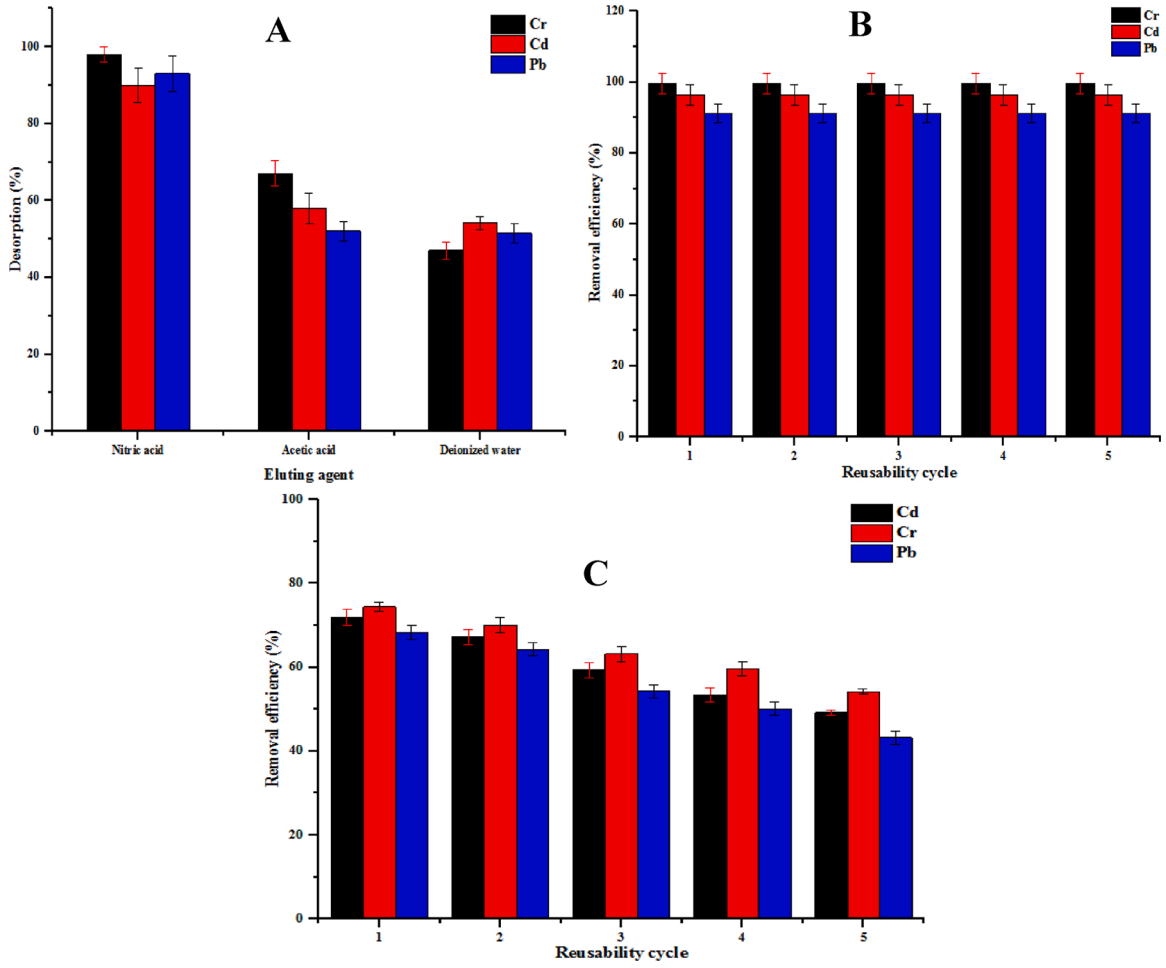

Fig. 12. (a) Desorption study of kaolin/TiO_2 nanoadsorbent after adsorption (b) Reusability cycles with 0.1 M EDTA for Cr, Cd and Pb removal (c) Reusability cycle without 0.1 M EDTA for Cr, Cd and Pb.

adsorption energy due to some mechanical contacts between the liquid-solid interfaces.

- The results provided from the various kinetic models employed showed good correlation coefficient and lowest Chi-square values of the pseudo-second order kinetic model, for the adsorption of pollutants.
- The Boyd and intra-particle diffusion model as the rate-determining steps control the adsorption process mechanism. Their plots do not pass through the origin, indicating some degree of boundary layer diffusion. This is attributed to chemical reaction through ion exchange, bulk, film and pore diffusion to the external surface of adsorbents.
- The thermodynamic parameters indicate that the adsorption process is spontaneous and endothermic. This result was supported by the increasing adsorption removal of the studied pollutants with an increase in temperature.

Author contributions

Mustapha S. carried out the experiments on the synthesized kaolin/TiO_2 nanocomposites and pollutant removal from wastewater. Some of the characterizations were performed by Shuaib DT and Mohammed AK. All authors contributed to writing and proofreading the paper.

Declaration of Competing Interest

Authors have declared that no competing interests exist.

Acknowledgements

The authors appreciate the financial support received from the Tertiary Education Trust Fund (TETFund) of Nigeria under a grant number TETFUND/FUTMINNA/2017/01.

References

Abukhadra, M.R., Mohamed, A.S., 2019. Adsorption removal of safranin dye contaminants from water using various types of natural zeolite. Silicon 11 (3), 1635–1647.
Ahmed, E., Abdulla, H.M., Mohamed, A.H., El-Bassuony, A.D., 2016. Remediation and recycling of chromium from tannery wastewater using combined chemical-biological treatment system. Process Saf. Environ. Prot. 104, 1–10.
Antonyová, A., Antony, P., 2017. Electro-flotation as the method of the water treatment in recycling process of contaminated water as an integral part of the reverse logistics system. Preprints, 2017120147.
APHA, 2005. Standard Methods for the Examination of Water and Wastewater, 21st ed. APHA American Public Health Association, Washington, D.C. 2005.
Barbooti, M.M., 2015. Simultaneous removal of chromium and lead from water by sorption on Iraqi Montmorillonite. J. Environ. Prot. (Irvine, Calif) 6 (03), 237.
Barbooti, M.M., Al-Dabbagh, B.D., Hilal, R.H., 2019. Preparation, characterization and utilization of polyacrylic acid–kaolin composite in the removal of heavy metals from water. Int. J. Environ. Sci. Technol. 16 (8), 4571–4582.
Belvera, C., Hanb, C., Rodrigueza, H.J.J., Dionysiou, D.D., 2016. Innovative W-doped titanium dioxide anchored on clay for photocatalytic removal of atrazine. Catal. Today.
Brito, G.C.B., Lange, L.C., Santos, V.L., Amaral, M.C.S., Moravia, W.G., 2019. Long-term evaluation of membrane bioreactor inoculated with commercial bakers' yeast treating landfill leachate: pollutant removal, microorganism dynamic and membrane fouling. Water Sci. Technol. 79 (2), 398–410.
Burakov, A.E., Galunin, E.V., Burakova, I.V., Kucherova, A.E., Agarwal, S., Tkacheva, A. G., Gupta, V.K., 2018. Adsorption of heavy metals on conventional and nanostructured materials for wastewater treatment purposes: a review. Ecotoxicol. Environ. Safety 148, 702–712.
Burham, N., Sayed, M., 2016. Adsorption behavior of Cd^{2+} and Zn^{2+} onto natural Egyptian bentonitic clay. Minerals 6 (4), 129.
Byambaa, M., Dolgor, E., Shiomori, K., Suzuki, Y., 2018. Removal and Recovery of Heavy Metals from Industrial Wastewater by Pecipitation and Foam Seperation Using Lime and Casein. J. Environ. Sci. Technol. 11, 1–9.
Dale, A.L., Casman, E.A., Lowry, G.V., Lead, J.R., Viparelli, E., Baalousha, M., 2015. Modeling nanomaterial environmental fate in aquatic systems. Environ. Sci. Technol. 49 (5), 2587–2593.
Dariania, R.S., Esmaeilia, A., Mortezaalia, A., Dehghanpour, S., 2016. Photocatalytic reaction and degradation of methylene blue on TiO_2 nano-sized particles. Optik 127, 714–7154.
Deng, L., Shi, Z., Luo, L., Chen, S., Yang, L., Yang, X., Liu, L., 2014. Adsorption of hexavalent chromium onto kaolin clay based adsorbent. J. Cent. South Univ. 21 (10), 3918–3926.
El-Naggar, I.M., Ahmed, S.A., Shehata, N., Sheneshen, E.S., Fathy, M., Shehata, A., 2019. A novel approach for the removal of lead (II) ion from wastewater using Kaolinite/Smectite natural composite adsorbent. Appl. Water Sci. 9 (1), 7–19.
Flory, P.J., 1956. Phase diagrams of rod-like polymer solution. Proceeding of Royal Society, London, Ser. A: Mathematical. Phys. Eng. Sci. 234, 73–89.
Foroutan, R., Peighambardoust, S.J., Mohammadi, R., Omidvar, M., Sorial, G.A., Ramavandi, B., 2020. Influence of chitosan and magnetic iron nanoparticles on chromium adsorption behavior of natural clay: adaptive neuro-fuzzy inference modeling. Int. J. Biol. Macromol. 151, 355–365.
Halsey, G., 1948. Physical adsorption on non-uniform surface. J. Chem. Phys. 16, 931–937.
Jovanovic, D.S., 1969. Physical adsorption of gases I: isotherms for monolayer and multilayer adsorption. Colloid Polymer Sci. 235, 1203–1214.
Kariim, I., Abdulkareem, A.S., Tijani, J.O., Abubakre, O.K., 2020. Development of MWCNTs/TiO_2 nanoadsorbent for Simultaneous removal of Phenol and Cyanide from refinery wastewater. Scientific African, e00593.
Khayyun, T.S., Mseer, A.H., 2019. Comparison of the experimental results with the Langmuir and Freundlich models for copper removal on limestone adsorbent. Appl. Water Sci. 9 (8), 170–177.
Kushwaha, A., Rani, R., Patra, J.K., 2020. Adsorption kinetics and molecular interactions of lead [Pb (II)] with natural clay and humic acid. Int. J. Environ. Sci. Technol. 17 (3), 1325–1336.
Li, Z., Pan, Z., Wang, Y., 2019. Enhanced adsorption of cationic Pb (II) and anionic Cr (VI) ions in aqueous solution by amino-modified nano-sized illite-smectite clay. Environ. Sci. Pollut. Res. Int. 26 (11), 11126–11139.
Lin, K., Lin, Y., Cheng, Y., Haung, Y., 2018. Preparation and characterization of V-Loaded titania nanotubes for adsorption/photocatalysis of basic dye and environmental hormone contaminated wastewaters. Catal. Today 307, 119–130.
Liu, Z., Wang, R., Kan, F., Jiang, F., 2014. Synthesis and characterization of TiO_2 nanoparticles. Asian J. Chem. 26 (3), 655–659.
Lofrano, G., Carotenuto, M., Libralato, G., Domingos, R.F., Markus, A., Dini, L., Gautam, R.K., Baldantoni, D., Rossi, M., Sharma, S.K., Chattopadhyaya, M.C., Giugni, M., Meric, S., 2016. Polymer functionalized nanocomposites for metals removal from water and wastewater: an overview. Water Res. 92, 22–37.
Lu, H., Wang, J., Wang, T., Wang, N., Bao, Y., Hao, H., 2017. Crystallization techniques in wastewater treatment: an overview of applications. Chemosphere 173, 474–484.
Ma, J., Chen, Y., Nie, J., Ma, L., Huang, Y., Li, L., Liu, Y., Guo, Z., 2018. Pilot-scale study on catalytic ozonation of bio-treated dyeing and finishing wastewater using recycled waste iron shaving as a catalyst. Sci. Rep. 8, 7555.
Madejova, J., 2003. FTIR techniques in clay mineral studies. Vib. Spectrosc. 31 (1), 1–10.
Maučec, D., Šuligoj, A., Ristić, A., Dražić, G., Pintar, G., Tušar, N.N., 2017. Titania versus zinc oxide nanoparticles on mesoporous silica supports as photocatalysts for removal of dyes from wastewater at neutral pH. Catal. Today 310, 32–41.
Mekatel, E., Amokrane, S., Aid, A., Nibou, D., Trari, M., 2015. Adsorption ofmethyl orange on nanoparticles of a synthetic zeolite NaA/CuO. ComptesRendus Chimie 18, 336–344.
Mishra, A., Mehta, A., Sharma, M., Basu, S., 2017. Enhanced heterogeneous photodegradation of VOC and dye using microwave synthesized TiO_2 /Clay nanocomposites: A comparison study of different type of clays. J. Alloys. Compd. 694, 574–580.
Oun, A., Tahri, N., Mahouche-Chergui, S., Carbonnier, B., Majumdar, S., Sarkar, S., Sahoo, G.C., Amar, R.B., 2017. Tubular ultrafiltration ceramic membrane based on titania nanoparticles immobilized on macroporous clay-alumina support: Elaboration, characterization and application to dye removal. Sep. Purification Technol. 188, 126–133.
Qian, H., Hu, Y., Liu, Y., Zhou, M., Guo, C., 2012. Electrostatic self-assembly of TiO_2 nanoparticles onto carbon spheres with enhanced adsorption capability for Cr(VI). Mater. Letters 68, 174–177.
Rao, R.A.K., Kashifuddin, M., 2016. Adsorption studies of Cd (II) on ball clay: comparison with other natural clays. Arab. J. Chem. 9, S1233–S1241.
Redlich, O., Peterson, D.L., 1959. A useful adsorption isotherm. J. Phys. Chem. 63 (1959), 1024–1026.
Setthaya, N., Chindaprasirt, P., Yin, S., Pimraksa, K., 2017. TiO_2-zeolite photocatalysts made of metakaolin and rice husk ash for removal of methylene blue dye. Powder Technol. 313, 417–426.
Sharaf El-Deen, S.E.A., Zhang, F.S., 2016. Immobilisation of TiO_2-nanoparticles on sewage sludge and their adsorption for cadmium removal from aqueous solutions. J. Exp. Nanosci. 11 (4), 239–258.
Sharififard, H., Ghorbanpour, M., Hosseinirad, S., 2018. Cadmium removal from wastewater using nano-clay/TiO_2 composite: kinetics, equilibrium and thermodynamic study. Adv. Environ. Technol. 4 (4), 203–209.
Sharma, A., Karn, R.K., Pandiyan, S.K., 2014. Synthesis of TiO_2 nanoparticles by sol-gel method and their characterization. J. Basic Appl. Eng. Res. 1 (9), 1–5.
Taghlidabad, R.H., Sepehr, E., Khodaverdiloo, H., Samadi, A., Rasouli-Sadaghiani, M.H., 2020. Characterization of cadmium adsorption on two cost-effective biochars for water treatment. Arab. J. Geosci. 13, 448–457.
Thaçi, B.S., Gashi, S.T., 2019. Reverse Osmosis Removal of Heavy Metals from Wastewater Effluents Using Biowaste Materials Pretreatment. Polish J. Environ. Studies 28 (1), 337–341.
Tijani, J.O., Momoh, U.O., Salau, R.B., Bankole, M.T., Abdulkareem, S.A., Roos, W.D., 2019. Synthesis and characterization of $Ag_2O/B_2O_3/TiO_2$ ternary nanocomposites for photocatalytic mineralization of local dyeing wastewater under artificial and natural sunlight irradiation. Environ. Sci. Pollut. Res. 26, 19942–19967.

Uddin, M.K., 2016. A review on the adsorption of heavy metals by clay minerals, with special focus on the past decade. Chem. Eng. J. 308, 438–462.

UNDESA (United Nations Department of Economic and Social Affairs), 2013. World Population Prospects: The 2012 Revision. New York, Population Division, United Nations (UN). http://esa.un.org/wpp/.

Wang, M., Wang, Z., Zhou, X., Li, S., 2019. Efficeient Removal of Heavy Metal Ions in Wastewater by Using a Novel Alginate-EDTA Hybrid Aerogel. Appl. Sci. 9, 547.

WHO, 2016. The Global Health Observatory (GHO) Is WHO's Portal Providing Access to Data and Analyses for Monitoring the Global Health Situation. See: http://www.who.int/gho/en/, accessed 16 April 2016.

Wongso, V., Chen, C.J., Razzaq, A., Kamal, N.A., Sambudi, N.S., 2019. Hybrid kaolin/TiO_2composite: Effect of urea addition towards an efficient photocatalyst for dye abatement under visible light irradiation. Appl. Clay Sci. 180, 105158.

Zou, C., Jiang, W., Liang, J., Guan, Y., Sun, X., 2019. Desorption Regeneration Performance of Magnetic Bentonite after Pb (II) Adsorbed. ChemistrySelect 4 (4), 1306–1315.

Zulfikar, M.A., Afrita, S., Wahyuningrum, D., Ledyastuti, M., 2016. Preparation of Fe_3O_4-chitosan hybrid nano-particles used for humic acid adsorption. Environ. Nanotechnol. Monitor. Manage. 6, 64–75.